Adaptation of pancreatic cancer cells to nutrient deprivation is reversible and requires glutamine synthetase stabilization by mTORC1

Pei-Yun Tsai[1,2], Min-Sik Lee[1,2,3], Unmesh Jadhav[4,5,6,7], Insia Naqvi[1], Shariq Madha[4,5], Ashley Adler[1,3], Meeta Mistry[8], Caroline A. Lewis[9], Daniel S. Hitchcock[3], Frederick R. Roberts[10], Peter DelNero[1,11], Thomas Hank[12], Kim C. Honselmann[12], Vicente Morales Oyarvide[4], Mari Mino-Kenudson[13], Clary B. Clish[3], Ramesh A. Shivdasani[4,5,6,7,14], and Nada Y. Kalaany[1,2,3*]

[1]Division of Endocrinology and Research Center for Metabolic Health, Boston Children's Hospital, Boston, MA, USA.
[2]Department of Pediatrics, Harvard Medical School, Boston, MA, USA.
[3]Broad Institute of MIT and Harvard, Cambridge, MA, USA.
[4]Department of Medical Oncology, Dana-Farber Cancer Institute, Boston, MA, USA.
[5]Center for Functional Cancer Epigenetics, Dana-Farber Cancer Institute, Boston, MA, USA.
[6]Department of Medicine, Brigham and Women's Hospital, Boston, MA, USA.
[7]Department of Medicine, Harvard Medical School, Boston, MA, USA.
[8]Bioinformatics Core, Harvard T.H. Chan School of Public Health, Boston, MA, USA.
[9]Whitehead Institute for Biomedical Research, Cambridge, MA, USA.
[10]FUJIFILM VisualSonics Inc., Toronto, ON, Canada.
[11]Cancer Prevention Fellowship Program, Division of Cancer Prevention, National Cancer Institute, Bethesda, MD, USA.
[12]Department of Surgery, Massachusetts General Hospital and Harvard Medical School, Boston, MA, USA.
[13]Department of Pathology, Massachusetts General Hospital and Harvard Medical School, Boston, MA, USA.
[14]Harvard Stem Cell Institute, Cambridge, MA, USA.
*email: nada.kalaany@childrens.harvard.edu

Abstract

Pancreatic ductal adenocarcinoma (PDA) is a lethal, therapy-resistant cancer that thrives in a highly desmoplastic, nutrient-deprived microenvironment. Several studies investigated the effects of depriving PDA of either glucose or glutamine alone. However, the consequences on PDA growth and metabolism of limiting both preferred nutrients have remained largely unknown. Here, we report the selection for clonal human PDA cells that survive and adapt to limiting levels of both glucose and glutamine. We find that adapted clones exhibit increased growth *in vitro* and enhanced tumor-forming capacity *in vivo*. Mechanistically, adapted clones share common transcriptional and metabolic programs, including amino acid use for *de novo* glutamine and nucleotide synthesis. They also display enhanced mTORC1 activity that prevents the proteasomal degradation of glutamine synthetase (GS), the rate-limiting enzyme for glutamine synthesis. This phenotype is notably reversible, with PDA cells acquiring alterations in open chromatin upon adaptation. Silencing of GS suppresses the enhanced growth of adapted cells and mitigates tumor growth. These findings identify non-genetic adaptations to nutrient deprivation in PDA and highlight GS as a dependency that could be targeted therapeutically in pancreatic cancer patients.

Introduction

With a steady rise in incidence and a poor 5-year survival rate of ~ 9%, PDA is now the third leading cause of cancer death in the US[1, 2]. Oncogenic *KRAS* mutations are highly prevalent in PDA (> 90%), driving many of its distinctive metabolic features[3, 4]. These include the macropinocytic uptake of extracellular macromolecules, the recycling of intracellular components[5-7], and the re-direction of glycolytic and glutaminolytic intermediates into anabolic and redox-controlling pathways required for PDA growth[8, 9]. However, whether these alterations are sufficient to account for the ability of PDA to thrive in a seemingly hostile *in vivo* microenvironment, where abnormal vasculature and exuberant

53 stroma restrict nutrient access, remains unknown.

54 Because nutrient availability largely dictates metabolic behavior[10], the relevance of studying
55 tumor metabolism within the native environment has been recently underscored[11-15]. Although culture
56 media composition can be modulated to mimic circulating metabolite levels[16, 17], this modulation may
57 not accurately reflect the tumor metabolic microenvironment. In particular, levels of glucose and
58 glutamine, two of the most abundant and tumor-preferred nutrients in the circulation, can be limiting in
59 PDA tumors, compared to benign adjacent tissue[7], and significantly lower within tumor cores, compared
60 to the periphery[18, 19]. Paradoxically, both glucose and glutamine are routinely supplemented in culture
61 media at levels that are significantly higher than the circulation: 11mM glucose and 2mM glutamine in
62 RPMI compared to ~ 5.5mM glucose and 0.6mM glutamine in serum[20]. Although prior studies focused
63 on depriving tumor cells of either glucose or glutamine alone[9, 21-24], how PDA cells survive and
64 proliferate under limiting levels of both major nutrients is not well understood.

65 To investigate this, we selected for clonal PDA cells that survive and adapt to limiting levels of
66 both glucose and glutamine. We find that the adapted clones have enhanced proliferation *in vitro* and
67 tumor-forming capacity *in vivo*. They also share common signaling, transcriptional and metabolic
68 alterations that are acquired upon adaptation. These include a post-translational role for mTORC1
69 signaling in the stabilization of glutamine synthetase (GS), and the use of amino acids for the synthesis
70 of glutamine and nucleotides. Of note, this phenotype is reversible, implicating epigenetic alterations in
71 the adaptation process, and highlighting GS as a candidate for therapeutic targeting in pancreatic cancer.

72

73 **Results**

74 **PDA cells adapted to low glucose / low glutamine have enhanced growth *in vitro* and *in vivo***

75 To test whether pancreatic cancer cells can survive and adapt to harsh nutrient-deprived conditions, we

76 cultured seven human PDA cell lines (AsPC-1, BxPC-3, HPAC, MIA PaCa-2, PANC-1, SUIT-2 and
77 PA-TU-8988T, herein termed 8988T) in customized low glucose (0.5mM) and low glutamine (0.1mM),
78 medium (L-L). These modifications represent ~20-fold reduction from standard RPMI medium, herein
79 referred to as high glucose-high glutamine (H-H) and 5- to 10-fold decrease from human serum levels[20]
80 (Fig. 1a); both L-L and H-H media were supplemented with 10% dialyzed fetal bovine serum (FBS).
81 Consistent with the requirement of glucose and glutamine for PDA growth[8, 9], most PDA cells died
82 within two weeks of culture in L-L medium, despite media replenishment every 2-3 days. However, rare
83 surviving cells were observed in 2 of the 7 PDA cell lines, SUIT-2 and 8988T. These cells gradually
84 gave rise to adapted clones, 3 of which (A-C4, C-5 and C-6) were selected per cell line. Adapted clones
85 were then studied in comparison to non-adapted clones (NA-C1, C-2 and C-3), which were isolated
86 from the corresponding parental PDA lines grown under H-H conditions (Fig.1a). All clones were
87 subsequently passaged every 3-4 days for use in experiments.

88 To assess their *in vitro* growth potential, adapted and non-adapted cells were first subjected to a
89 7-day proliferation assay performed without media replenishment. Whereas no significant differences
90 were detected in H-H medium conditions (Supplementary Fig. 1a,b), adapted cells from both lines
91 showed enhanced proliferative capacity (Fig. 1b) and decreased cell death (Fig. 1c), compared to non-
92 adapted clones, in L-L medium. In a colony formation assay, adapted 8988T clones generated a larger
93 number of colonies independent of the medium, whereas adapted SUIT-2 clones tended to form more
94 colonies in L-L but not in H-H medium. (Fig. 1d and Supplementary Fig. 1c). When plated under 3-
95 dimensional (3-D) culture conditions, only adapted 8988T cells formed spheres independent of the
96 medium (Fig. 1e and Supplementary Fig. 1d-f). SUIT-2 clones formed a similar number of spheres,
97 independent of the medium or adaptation (Supplementary Fig. 1d,e). However, SUIT-2 spheres tended
98 to be larger in adapted, compared to non-adapted clones, when cultured under L-L, but not H-H

99 conditions (Fig. 1e and Supplementary Fig. 1f).

100 Because autophagy and macropinocytosis are well-recognized dependencies in PDA[3, 5, 6], we
101 assessed their potential contribution to the enhanced proliferation of the adapted clones under nutrient-
102 limiting conditions. No differential increase in autophagic flux was observed in the adapted cells,
103 compared to non-adapted controls in L-L medium (Supplementary Fig. 2a,b). Moreover, uptake of
104 tetramethylrhodamine (TMR)-labeled dextran, an indicator of macropinocytosis, was not further
105 increased in the adapted, compared to non-adapted cells, under L-L conditions (Supplementary Fig. 2c).
106 These data indicate that surviving PDA cells that adapt to chronic glucose and glutamine deprivation
107 acquire a proliferative potential that depends on processes other than autophagy or macropinocytosis.

108 To test whether the adaptation-mediated *in vitro* phneotype could be translated *in vivo*, adapted
109 and non-adapted 8988T PDA clonal cells were orthotopically injected into the pancreas of B6.Rag1$^{-/-}$
110 mice. Within the span of 33 days, only 1 out of 14 non-adapted cell injections derived from 2 distinct
111 clones formed a tumor (100 mm^3 in volume). In contrast, 14 of 14 adapted clonal cell injections
112 produced tumors that were larger in size, with average volumes of 600 mm^3 and 250 mm^3 for clones 4
113 and 5, respectively (Fig. 1f and Supplementary Fig. 1g). These results demonstrate that metabolic
114 adaptation to a nutrient-deprived environment can endow cancer cells with higher growth fitness,
115 allowing tumors to survive and thrive during periods of nutrient starvation.

116

117 **Adapted PDA clones display altered amino acid and nucleotide metabolism coupled with**
118 **enhanced mTORC1 signaling**

119 To identify transcriptional alterations that convey enhanced proliferative potential to PDA upon
120 adaptation to nutrient deprivation, we used RNA-Seq to profile transcripts in SUIT-2 and 8988T clones
121 under L-L conditions. Principal component analysis (PCA) of the 500 most variable genes indicated

122 significant segregation (83% variance) of non-adapted clones, based on cell type (Supplementary Fig.
123 3a). This was however minimized in adapted clones, which clustered together (8% variance), implying
124 induction of a common transcriptional adaptation program, independent of the genetic background.
125 Gene set enrichment analysis (GSEA) revealed significant enrichment in the adapted clones for
126 pathways involved in amino acid synthesis and degradation, as well as purine and pyrimidine synthesis
127 (Supplementary Fig. 3b).

128 Metabolic profiling of SUIT-2 and 8988T clones treated for 24 hours with H-H or L-L medium
129 yielded an adaptation signature that largely overlaps with the altered transcriptomes (Supplementary Fig.
130 4a,b). Compared to H-H, all clones under L-L conditions displayed markedly higher levels of
131 intracellular amino acids other than glutamine, glutamate and aspartate (Supplementary Fig. 4a),
132 consistent with glutamine deprivation and indicative of enhanced autophagy. This increase in amino
133 acids was significantly suppressed in the adapted clones, compared to non-adapted controls, suggesting
134 enhanced utilization of intracellular amino acids (Supplementary Fig. 4a). Furthermore, non-adapted
135 cells showed significant accumulation of nucleotides and their biosynthetic precursors, reflecting
136 decreased DNA synthesis. In contrast, the adapted clones displayed a nucleotide biosynthesis profile that
137 closely mirrors that of PDA clones under H-H conditions, consistent with enhanced proliferation. This
138 profile included lower levels of mono- and di-nucleotide phosphates, used to generate tri-nucleotide
139 phosphates, which differentially accumulate in the adapted clones (Fig. 2a and Supplementary Fig. 4).
140 Indeed, although *de novo* pyrimidine synthesis was higher under H-H compared to L-L conditions, a
141 differential increase upon adaptation was observed only under L-L conditions (Fig. 2b). This was
142 evident in doubling of ^{14}C incorporation into DNA, 40 hours after labeling of cells with ^{14}C-aspartate
143 (Fig. 2b).

144 Signaling downstream of the mammalian target of rapamycin complex 1 (mTORC1) can induce

145 *de novo* pyrimidine synthesis through activation of the rate-limiting enzyme carbamoyl-phosphate
146 synthetase 2, aspartate transcarbamoylase, dihydroorotase (CAD)[25]. We therefore investigated a role for
147 mTORC1 in the adaptation of the PDA clones to nutrient deprivation. Compared to non-adapted clones,
148 adapted SUIT-2 and 8988T cells showed increased phosphorylation levels of CAD on Serine 1859, a
149 site of ribosomal S6-Kinase (S6K1) activity (Fig. 2c). This increase was particularly striking under L-L
150 conditions, where non-adapted clones showed low (SUIT-2) to undetectable (8988T) CAD
151 phosphorylation. Importantly, this was mirrored by enhanced mTORC1 activity, as evidenced by
152 sustained phosphorylation of its downstream effectors S6K1 and 4E-binding protein (4E-BP1), despite
153 nutrient deprivation (Fig. 2c). On the other hand, AKT phosphorylation levels were decreased in adapted
154 cells consistent with mTORC1-AKT negative feedback loops[26-28] (Supplementary Fig. 5a).
155
156 **Adapted PDA clones have enhanced glutamine synthesis**
157 Glutamine is a pleiotropic amino acid required for protein synthesis and numerous anabolic reactions in
158 proliferating cells[21]. We therefore asked whether the adapted clones have induced *de novo* glutamine
159 synthesis under L-L conditions. mRNA levels of glutamine synthetase (GS, also termed GLUL), which
160 catalyzes the condensation of glutamate and ammonium to generate glutamine (Fig. 3a), were only
161 moderately increased in adapted clones derived from SUIT-2, but not 8988T cells (Supplementary Fig.
162 6a). However, GS protein levels were markedly induced in all adapted clones from both PDA cell lines,
163 compared to non-adapted controls (Fig. 3b), where GS levels either remained undetectable (8988T) or
164 were minimally detected (SUIT-2). This occurred only under L-L conditions, as no clones harbored
165 detectable levels of GS in H-H medium, independent of adaptation (Fig. 3b). Although these findings
166 are consistent with a glutamine-dependent post-translational regulation of GS[29, 30], it is noteworthy that
167 non-adapted clones only displayed a mild to no increase in GS levels 24 hours following exposure to L-

168 L medium (Fig. 3b), implying differential metabolic rewiring in the PDA clones upon adaptation to
169 prolonged glutamine deprivation. Importantly, GS protein levels were mirrored by its enzymatic activity
170 levels, as demonstrated by metabolic tracing of ^{15}N-ammonium chloride (NH_4Cl) in SUIT-2 cells (Fig.
171 3c). Because glutamate dehydrogenase (GDH, also termed GLUD) catalyzes the reductive amination of
172 alpha-ketoglutarate (α-KG) to generate glutamate (Fig. 3a), a moderate increase was observed in the
173 ^{15}N-glutamate fraction between H-H and L-L conditions in SUIT-2 cells (~18% vs 25%), independent of
174 adaptation (Fig. 3c). This suggested the use by the adapted cells of newly generated glutamate to
175 synthesize glutamine. Indeed, adapted clones cultured in L-L medium had a marked increase in ^{15}N-
176 glutamine (M+1) fraction, generated from either condensation of ^{15}N-ammonium and unlabeled
177 glutamate, or unlabeled ammonium and GDH-derived ^{15}N-glutamate, compared to non-adapted controls
178 (30% vs 8%, respectively). This increase was also observed in the (M+2) labeled fraction, which is
179 generated when both substrates are labeled (8% in adapted vs 2% in non-adapted cells). On the other
180 hand, ^{15}N-glutamine levels were either undetectable or minimally detected in the PDA clones under H-H
181 conditions, independent of adaptation (Fig. 3c). These data indicate that only PDA clones that survive
182 and adapt to long-term glutamine deprivation are able to induce GS protein levels under L-L conditions,
183 so as to increase GS-mediated glutamine synthesis.
184
185 **Adapted PDA cells use amino acids as a nitrogen source for glutamine and nucleotide synthesis**
186 In addition to reductive amination of α-KG through GDH (Fig. 3a), the transamination reaction
187 catalyzed by branched chain amino acid (BCAA) transaminase (BCAT2) could contribute to the
188 generation of mitochondrial glutamate that is then used for glutamine synthesis. Moreover, aspartate
189 transaminase (GOT2, also termed AST2) could transfer the nitrogen from glutamate to aspartate, a key
190 substrate in nucleotide biosynthesis (Fig. 3d). Global metabolite profiling of the PDA clones revealed a

191 significant decrease in amino acid levels, including the branched chain amino acids (BCAA) leucine,
192 valine and isoleucine in all adapted clones, suggesting enhanced amino acid utilization by the more
193 proliferative cells (Fig. 3e and Supplementary Fig. 4a). Although the PDA clones did not seem to share a
194 common transcriptional regulation of transaminases in both cell lines under L-L conditions
195 (Supplementary Fig. 6b), protein levels of BCAT2 and GOT2 were significantly increased in at least 2
196 of the 3 SUIT-2 and 8988T adapted clones (Supplementary Fig. 6c). ^{15}N-leucine tracing demonstrated
197 that the labeled nitrogen incorporates at significantly higher levels into glutamate, aspartate and
198 intermediates in nucleotide synthesis in adapted, compared to non-adapted clones under L-L conditions
199 (Fig. 3f and Supplementary Fig. 7a). Moreover, the ^{15}N-labeled fraction of glutamine was minimal (1%)
200 under nutrient-replete H-H conditions, whereas a marked 5-fold increase in ^{15}N-glutamine was detected
201 under L-L conditions, specifically in the adapted clones (Fig. 3f and Supplementary Fig. 7a). These data
202 imply that BCAAs are a significant source for *de novo* synthesis of glutamine and nucleotides in PDA
203 cells adapted to L-L conditions.
204
205 **mTORC1 activation and enhanced proliferative potential are reversible in adapted PDA clones**
206 Because the adapted clones sustain active mTORC1 signaling independent of nutrient deprivation, we
207 asked whether the adaptation process had selected for cells with inherent mutations that constitutively
208 activate mTORC1. We cultured the adapted clones in nutrient-replete H-H medium for 4 or more
209 consecutive passages (a process we termed "adaptation reversal") followed by treatment for 24 hours
210 with L-L medium (Fig. 4a). Reverse-adapted (RA) clones displayed gradual suppression of mTORC1
211 activity (Fig. 4b and Supplementary Fig. 8a,b), indicating that the enhanced anabolic signaling acquired
212 upon adaptation is unlikely to result from genetic mutations selected for in the adapted clones.
213 Importantly, *in vitro* survival and growth of adapted clones were partially reversed, with all RA clones

214 exhibiting decreased proliferation compared to adapted clones and two 8988T clones displaying
215 enhanced cell death (Fig. 4c,d and Supplementary Fig. 8c). Furthermore, among a pool of 1,842 genes
216 that were significantly up-regulated (≥3-fold, q <0.05) upon adaptation in both SUIT-2 and 8988T cells,
217 reversal was associated with partial suppression of this transcriptional response (Fig. 4e), consistent with
218 decreased mTORC1 signaling and proliferative capacity (Fig. 4b-d and Supplementary Fig. 8a-c).
219 These findings led us to investigate a potential epigenetic basis for PDA cells' adaptation to
220 nutrient deprivation. Assays for transposase-accessible chromatin with high throughput sequencing
221 (ATAC-seq) identified a significantly altered landscape of open chromatin in adapted clones, with gains
222 and losses of chromatin accessibility at thousands of genomic sites (Fig. 4f), including 3,807 enhancers
223 common to adapted 8988T and SUIT-2 clones (Supplementary Fig. 8d). Adaptation-induced changes in
224 chromatin accessibility correlated with gene expression changes in both lines (Fig. 4g and
225 Supplementary Fig. 8e). Among the 1,842 transcripts altered upon adaptation and linked to enhancers
226 modulated in both cell lines, gains of chromatin access and transcription outnumbered the losses (Fig.
227 4g). Notably, alterations in open chromatin were largely preserved in RA cells (Fig. 4f and
228 Supplementary Fig. 8f, left) and reversion was infrequent (Fig. 4f and Supplementary Fig. 8f, right),
229 indicating possible acquisition of epigenetic memory when PDA cells adapt robustly to nutrient
230 deprivation.
231
232 **mTORC1 prevents proteasomal degradation of GS in adapted PDA clones**
233 Because the induction of GS protein in adapted cells consistently mirrored mTORC1 signaling (Fig. 2c
234 and 3b), including reversibility upon de-adaptation (Fig. 4b and Supplementary Fig. 8a-b), we asked
235 whether mTORC1 regulates GS levels. Upon treatment with the mTOR kinase inhibitor Torin1, *GS*
236 mRNA levels were increased in adapted clones under L-L conditions (Supplementary Fig. 9a). In

237 contrast, consistent with post-transcriptional GS regulation, Torin1 markedly decreased GS protein
238 levels (Fig. 5a). This decrease was not observed upon treatment with cycloheximide, but only when
239 Torin1 was added to the cells, indicating that mTORC1 regulation of GS is post-translational (Fig. 5b
240 and Supplementary Fig. 9b). Indeed, whereas treatment with the proteasomal inhibitor MG-132 did not
241 significantly affect GS levels in adapted clones over 2-12 h, it induced GS in all non-adapted clones
242 under L-L conditions (Fig. 5c). Importantly, the Torin1-induced decrease in GS levels in adapted cells
243 was rescued upon treatment with MG-132 (Fig. 5d). Furthermore, mTORC1 inhibition promoted GS
244 poly-ubiquitination, as evidenced in immunoprecipitated GS from adapted cells co-treated with Torin1
245 and MG-132 (Fig. 5e). Altogether, these data demonstrate that GS is ubiquitinated and targeted for
246 proteasomal degradation in non-adapted clones, even under L-L conditions, and that mTORC1 prevents
247 this degradation, leading to GS stabilization in adapted clones.
248
249 **PDA cells adapted to nutrient-deprived conditions are sensitive to GS inhibition**
250 To assess the contribution of glutamine synthesis to the enhanced growth of the adapted cells, PDA
251 clones were treated with the GS inhibitor L-methionine sulfoximine (MSO). Adapted cell proliferation
252 was mitigated under L-L, but not H-H conditions, underscoring the relevance of glutamine synthesis in
253 the nutrient-deprived state (Supplementary Fig. 10a). Genetic silencing of GS similarly suppressed
254 adapted cell proliferation and colony formation (Fig. 6a-c, Supplementary Fig. 10b,c). To ask whether
255 the contribution of GS to enhanced *in vitro* PDA growth extends *in vivo*, we induced knockdown of GS
256 in orthotopic PDA transplants (Fig. 6d,e). Five days following injection of adapted 8988T expressing
257 control or *GS* hairpins into the pancreas, gene silencing was induced by treating mice with doxycycline
258 (Dox) in the drinking water. Two distinct *GS* hairpins attenuated PDA growth (Fig. 6d and
259 Supplementary Fig. 10e,f), resulting in 6.1- to 9.2-fold lower tumor weights upon Dox treatment (Fig.

260 6d). These findings indicate that GS-mediated glutamine synthesis is required for PDA cells to survive
261 and adapt to the characteristic nutrient-deprived PDA environment and highlight GS as a metabolic
262 target in treating pancreatic cancer (Fig. 6f).

263 To extend our findings to human pathology, tissue microarrays (TMAs) of resected tumors from
264 127 pancreatic cancer patients were immunostained and scored for GS protein levels. As a reference for
265 intensity, stained control cores of normal pancreas showed high GS levels in islets and modest levels in
266 acinar cells. Within tumor cores, PDA cells displayed heterogeneous cytoplasmic staining that varied
267 widely from strong to moderate to weak, with an overall score lower than that of acinar cells. As a
268 result, no significant association was found between PDA GS levels and tumor size, lymph node
269 involvement (pT or pN staging, the American Joint Commission on Cancer, AJCC 8th edition[31]) or
270 patient survival (Supplementary Fig. 11a-c) Although these results seem discordant with a recent report
271 that GS expression is a feature of *KRAS*-driven PDA[32], the pathological heterogeneity and variability in
272 GS protein levels is consistent with an inverse correlation with nutrient deprivation (Figs. 3, 4 and
273 Supplementary Fig. 8). Indeed, nutrient distribution is recognized to be heterogeneous in the tumor
274 microenvironment, with glutamine levels being most depleted within tumor cores, compared to the
275 periphery[18, 19]. Therefore, gradients of GS protein levels may exist among distinct PDA cell clusters
276 within the tumor mass, depending on their precise location and proximity to blood vessels. Nevertheless,
277 based on our results and those of Bott *et al.*[32], targeting GS in the nutrient-deprived PDA tumors holds
278 significant therapeutic value in pancreatic cancer.

279

280 **Discussion**

281 The *in vitro* dependence of proliferating cells on glutamine[21] was recently questioned in the *in vivo*
282 setting, where tumors preferably utilize glucose and other metabolites, rather than circulating glutamine,

283 as sources of tricarboxylic acid (TCA) cycle carbon[13, 33-35]. This observation is supported by *in vivo*
284 resistance of tumors to inhibitors of glutaminolysis[36]. Differences in nutrient levels between cell culture
285 media and human serum, in addition to the *in vivo* tumor environment, might partially explain this
286 discrepancy[11, 37]. However, although glutamate is a major source of TCA cycle carbon and nitrogen for
287 transamination reactions and glutathione synthesis, glutamine *per se* is required for protein synthesis and
288 is an indispensable source of amide nitrogen for nucleotide and hexosamine synthesis. Therefore,
289 whereas proliferating tumor cells may resort to alternative sources of glutamate, such as transamination
290 reactions instead of glutaminolysis, they can only survive in glutamine-deprived conditions if they can
291 synthesize glutamine *de novo*.

292 Moreover, although glutamine may not seem to be depleted in extracts of whole tumors or tumor
293 interstitial fluid[15], tumor cores hold lower levels than the periphery[18, 19]. Thus, the precise location of a
294 cancer cell within the hypoxic, stromally dense tumor may dictate its dependence on glutamine at
295 various times. Distinct clusters of tumor cells likely exist within PDA tumors with differential nutrient
296 access depending on the proximity to blood vessels and density of the surrounding stroma. The
297 deprivation of PDA tumor cells of nutrients may also change over time, as tumor growth reshapes 3D
298 cellular organization and the proximity of cancer cells to stroma and endothelial cells. It is therefore not
299 surprising that, unlike Bott *et al.*[32], we found no significant association between average GS levels and
300 tumor grade or patient survival (Supplementary Fig. 11). We find instead that rare clonal cells are able
301 to survive and adapt to low levels of the tumor-preferred nutrients glucose and glutamine; these cells
302 induce glutamine synthesis, which is required for their growth *in vitro* and *in vivo*.

303 Despite chronic nutrient deprivation in the adapted cells, we find that activated mTORC1
304 induces GS. Although GS is known to be regulated post-translationally[29, 30], the signaling basis for this
305 regulation was unknown. We show that mTORC1 plays a key post-translational role in stabilizing GS by

306 preventing its ubiquitination and proteasomal degradation. mTORC1 inhibition was previously shown to
307 enhance proteasomal degradation of long-lived proteins[38], but GS was not identified as a specific target,
308 perhaps because the experiments were performed under glutamine-replete conditions. What induces
309 mTORC1 activity in the absence of glucose and glutamine in adapted PDA cells is a question worthy of
310 future investigation. One plausible explanation is that epigenetic alterations that occur upon adaptation
311 to nutrient deprivation (Fig. 4 and Supplementary Fig. 8) may influence genes that directly or indirectly
312 activate mTORC1.

313 We propose that PDA cells that survive and adapt to nutrient deprivation acquire an epigenetic
314 state that endows them with the flexibility to switch between metabolic states that are optimal for growth
315 under nutrient-replete or nutrient-deprived conditions. A key contributing factor to the adaptation to
316 nutrient-depleted conditions is activation of mTORC1, which in turn stabilizes GS, thus enabling
317 essential glutamine synthesis for pancreatic cancer growth (Fig. 6f). Consequently, targeting of GS,
318 which expression is induced in nutrient-deprived cell clusters within PDA tumors, holds therapeutic
319 benefit to pancreatic cancer patients.

320

321 **Methods**

322 **Reagents.** Antibodies for western blotting were from Abcam: BCAT1 (ab107191), GOT2 /
323 FABP-1 (ab171739); BD Biosciences: GS / GLUL (BD-61057); Cell Signaling Technology
324 (CST): AKT (pan, C67E7, # 4691), pS473-AKT (193H12, # 4058), pT308-AKT (244F9, #
325 4056), BCAT2 (# 9432), CAD (# 11933), pS1859-CAD (# 12662), 4EBP1 (53H11, # 9644),
326 pS65-4EBP1 (# 9451), LC3B (# 2775), pThr389-S6K (# 9234); Novus Biologicals: GOT1
327 (NBP1-54778); Proteintech: GLUD1 / GDH1 (14299-1-AP); Santa Cruz Biotechnology: S6Kα
328 (H-9, sc-8418), GAPDH (FL-335, sc-25778), β-Actin (sc-47778). All western blot antibodies

329 were used at 1:1,000 dilution, except for β-Actin (1: 20,000). Antibodies for
330 immunoprecipitation, ubiquitination or immunohistochemistry are described in the respective
331 Methods sections below. Chloroquine (Sigma-Aldrich, C6628); Cycloheximide (Sigma-Aldrich,
332 C4859); DMSO (Sigma-Aldrich D2650); MG-132 (Selleck Chemicals, S2619); Doxycycline
333 (Sigma-Aldrich; D9891); L-Methionine Sulfoximine, MSO (Sigma-Aldrich; M5379); Torin 1
334 (Selleck Chemicals, S2827).
335
336 **Cell culture.** Human PDA cell lines were from the American Type Culture Collection or ATCC
337 (AsPC-1, BxPC-3, HPAC, MIA PaCa-2, PANC-1), Japanese Collection of Research
338 Bioresources (SUIT-2), or the German Collection of Microorganisms and Cell Cultures (PA-TU-
339 8988T) and were authenticated by STR profiling at ATCC. All cell lines tested negative for
340 mycoplasma using LookOut Mycoplasma PCR Kit (Sigma, MP0035). All cells were maintained
341 at 37 °C in a humidified incubator with 5% CO2 and were grown in media supplemented with
342 10% dialyzed fetal bovine serum (Sigma-Aldrich F0392). For adaptation or reverse adaptation to
343 "low glucose, low glutamine" (L-L) medium, PDA cells were cultured in RPMI 1640 medium
344 lacking both glucose and L-glutamine (US Biological, R9011-01) that was supplemented with
345 0.5 mM glucose (Thermo Fisher Scientific, A2494001) and 0.1 mM glutamine (Thermo Fisher
346 Scientific, 25030-81). Non-adapted cells were cultured in the same RPMI 1640 medium that was
347 however supplemented with 11mM glucose and 2 mM glutamine, and was termed "high glucose,
348 high glutamine" (H-H) medium.
349
350 **Gene knockdown.** For small interfering RNA knockdown, ON-TARGETplus Human GS
351 (GLUL) siRNA with target sequence: GCACACCUGUAAACGGAUA (J-008228-09) or control

352 non-targeting siRNA: UGGUUUACAUGUUGUGUGA (D-001810-02-05) were purchased from
353 Dharmacon, Horizon Discovery (Cambridge, UK) and transfected according to the
354 manufacturer's protocol. For generation of PDA cells with stable doxycycline-inducible GS or
355 control (Scramble) knockdown, the corresponding hairpins were cloned into Tet-pLKO-puro
356 plasmid (21915; Addgene). Lentiviral supernatants were generated by transfecting the plasmids
357 into 293T cells and used to infect 8988T cells that were then selected for at least 7 days with 2
358 $\mu g\ ml^{-1}$ puromycin (Sigma-Aldrich, P8833). The RNAi consortium clone IDs for the hairpins
359 used were: shGS #1 (G05) TRCN0000343992 (CACACCTGTAAACGGATAATG); shGS #2
360 (G06) TRCN0000344059 (ATAACCACTGCTTCCATTTAA); Control Scramble shRNA
361 sequence (CCTAAGGTTAAGTCGCCCTCGCTCGAGCGAGGGCGACTTAACCTTAGG)
362 was the same as that from Addgene Plasmid # 1864.
363
364 **Cell proliferation and cell death assays.** Cells were seeded on day 0 in their respective
365 maintenance culture medium in 96-well plates, at a density of 3,000 cells per well, and incubated
366 overnight. On day 1, the cells were washed once with phosphate buffered saline (PBS) and
367 incubated in their experimental medium supplemented with propidium iodide (2 $\mu g\ ml^{-1}$) for up
368 to 7 days. Live and dead cells were counted on the indicated days using the Celigo Image
369 Cytometer (Nexcelom Bioscience), and either normalized to day 1 (live cell proliferation
370 curves), or presented as percentage of propidium iodide-positive cells per total cell number (cell
371 death).
372
373 **Clonogenic assay.** 600 cells were seeded per well in 6-well plates in their appropriate
374 maintenance medium and incubated overnight. The next day, cells were washed once with PBS

375 and incubated in their experimental medium for 7-10 days. Colonies were then either directly
376 counted using the Celigo Image Cytometer (Nexcelom Bioscience), or first stained and then
377 counted using the following protocol: media were removed and the cells fixed in a solution of
378 0.2% Crystal Violet (Sigma-Aldrich, C0775) in 80% methanol for 15-30 min. The wells were
379 then washed in distilled water and allowed to dry overnight, before colonies were counted using
380 the Celigo Image.
381
382 **Sphere formation assay.** 50 cells were seeded per well in 96-well plates and incubated
383 overnight in their appropriate maintenance medium supplemented with 4% matrigel (Corning,
384 356231). The next day, cells were washed once gently with PBS and treated with the
385 experimental medium. Spheres were counted after 7-10 days using the Celigo Image Cytometer
386 (Nexelcom Bioscience).
387
388 **Macropinocytosis assay.** Cells were seeded onto glass coverslips (Bellco Glass, 1943-10012A)
389 in 24-well plates and incubated overnight in their maintenance culture medium. The next day, the
390 medium was replaced with fresh L-L medium containing 10% dialyzed FBS, and the cells were
391 incubated for 24 h. Macropinosomes were assayed as previously described[39] and outlined below.
392 70-kDa TMR-dextran (Thermo Fisher Scientific, D1818) was added to the cells at a final
393 concentration of 1 mg ml^{-1} and the cells incubated for 30 min at 37°C, in the absence or presence
394 of 25 μM EIPA (Sigma-Aldrich; A3085). Cells were then rinsed 3 times on ice with ice-cold
395 PBS and immediately fixed in 4% paraformaldehyde (EMS, 15710-S) for 30 min. After staining
396 the cells with 1 μg ml^{-1} DAPI (Thermo Scientific, D3571) in PBS for 15min, the coverslips were
397 mounted onto glass slides (VWR, 48311-703) using Fluoroshield mounting medium (Sigma,

398 F6182). Image acquisition was performed using a Nikon Eclipse 90i Advanced Automated
399 Research Microscope equipped with a standard optical filter set including DAPI and
400 Rhodamine/Texas Red. Images were captured with a 40x objective and the NIS-Elements
401 Advanced Research Microscope Imaging Software (Nikon). Exposure time for DAPI acquisition
402 was 100 ms and that for TMR acquisition was 400 ms. Representative images were captured in
403 at least 3 different fields per well in duplicate wells, per condition and analyzed using ImageJ
404 software (NIH). At least 200 cells were counted per condition. Macropinosomes were visualized
405 after setting the threshold of the "Auto Contrast" feature in Image J to 134. The number and area
406 of labeled macropinosomes were then determined using the "Analyze Particles" feature, and
407 macropinocytic uptake was computed by the total particle number and area per cell.
408
409 **U-^{14}C-asparate incorporation into DNA**
410 Cells were seeded overnight (57,000 per well) in 6-well-plates with triplicate wells per condition.
411 The cells were then washed twice with PBS and incubated with either H-H or L-L medium
412 supplemented with 1μCi per well of L-[U-^{14}C]-Aspartic acid (PerkinElmer,
413 NEC268E050UC) for 40 h. The cells were washed twice with PBS before DNA was extracted
414 using PureLink® Genomic DNA Mini Kit (Thermo Fisher-K182001) and quantified using a
415 spectrophotometer. Equal volumes of DNA were added to scintillation vials and radioactivity
416 was measured by liquid scintillation counting and normalized to total DNA concentration.
417
418 **Immunoblotting.** For western blotting, cells were rinsed once in ice-cold PBS and collected in
419 lysis buffer containing 50 mM HEPES KOH, pH 7.4, 40mM NaCl, 2mM EDTA, 1.5mM
420 orthovanadate, 50mM NaF, 10mM pyrophosphate, 10mM glycerophosphate, EDTA-free

421 protease inhibitors (Thermo Fisher Scientific, 88266) and 1% Triton X-100. Proteins from total
422 lysates were resolved by 8–12% SDS–PAGE, transferred to polyvinylidene difluoride (PVDF)
423 and the blot was exposed to film.
424
425 **Immunoprecipitation and ubiquitination assay.** To assess GS protein ubiquitination, cells
426 were treated with either control vehicle DMSO or MG132 (10 μM) for 8 h. Cells were then lysed
427 under denaturing conditions using the lysis buffer (40 mM HEPES KOH, pH 7.4, 1% SDS)
428 containing 5 mM N-ethylmaleimide (NEM, Sigma-Aldrich, E1275) to prevent deubiquitination
429 and boiled for 5 min. The lysates were diluted 10-fold in IP buffer (40 mM HEPES KOH pH 7.4,
430 50 mM NaF, 10 mM Sodium pyrophosphate, 10 mM Sodium beta-glycerophosphate, 1.5 mM
431 Sodium Orthovanadate, 2.5 mM MgCl2, EDTA-free protease inhibitors, and 0.5% Triton X-
432 100). IP was performed by incubating the samples with 2 μg of normal rabbit IgG control (Santa
433 Cruz, sc-2027) or 2μg GS antibody (Abcam, ab73593) overnight with rotation at 4°C. Protein G
434 agarose bead slurry (Invitrogen, 15920-010) was added to the pre-cleared lysates (60 μl, 50:50)
435 and incubated with rotation for 1.5-2 hr at 4°C. The beads were then washed once with IP buffer,
436 followed by 3 additional washes with IP buffer supplemented with 500 mM NaCl. Loading
437 buffer was added to the immunoprecipitated proteins, which were then boiled, resolved by SDS-
438 PAGE and transferred to a PVDF membrane. Ubiquitinated GS was identified by HRP-
439 conjugated anti-Ubiquitin antibody (1:5,000; Enzo Life Sciences, FK2, BML-PW0150-0100).
440
441 **Quantitative real-time PCR.** Total mRNA was isolated with RNA STAT-60 (Tel-Test, Cs-111)
442 according to the manufacturer's instructions, treated with DNase I (RNase-free, Roche
443 Molecular Biochemicals**,** 04716728001) and reverse-transcribed into cDNA with random

444 hexamers using the SuperScript II First-Strand Synthesis System (Invitrogen, 18064071).
445 Primers listed below were validated and PCR reactions performed as previously described[40].
446 Quantitative PCR reactions were performed in triplicates using an Applied Biosystems ViiA 7
447 Real-Time PCR system. PCR reactions contained cDNA resulting from reverse transcription of
448 25ng total RNA, 150nM of each primer and 5 μl 2X-Jump Start SYBR Green PCR Mix
449 (Invitrogen) in10 μl total volume. Relative mRNA levels were calculated using the comparative
450 CT method and normalized to cyclophilin. The QPCR primers used were:
451 *BCAT1*: 5'-GTGGAGTGGTCCTCAGAGTTT-3' and 5'-AGCCAGGGTGCAATGACAG-3'
452 *BCAT2*: 5'-GCTCAACATGGACCGGATG-3' and 5'-CCGCACATAGAGGCTGGTG-3'
453 *CyclophilinA* (CYPA): 5'-GGAGATGGCACAGGAGGAA-3' and 5'-
454 GCCCGTAGTGCTTCAGCTT-3'
455 *GOT1*: 5'-ATTTCTTAGCGCGTTGGTACA-3' and 5'-ACACAGCATTGTGATTCTCCC-3'
456 *GOT2*: 5'-AGCCTTACGTTCTGCCTAGC-3' and 5'- AAACCGGCCACTCTTCAAGAC-3'
457 *GS*: 5'-AAGAGTTGCCTGAGTGGAATTTC-3' and 5'-AGCTTGTTAGGGTCCTTACGG-3'.
458
459 **RNA-Seq sample preparation**: Cells were seeded overnight at 700,000 per 10 cm plate. The
460 cells were then washed once with PBS and incubated in L-L medium for 24 h. RNA was
461 isolated and purified using miRNeasy Mini Kit (Qiagen-217004). Total RNA (> 150 ng) was
462 sent to the Broad Institute Genomics Platform for library preparation. RNA quality and insert-
463 size was assessed by Caliper LabchipGXII producing a RQS value (equivalent to RIN). RNA
464 quantity was determined by PicoGreen. mRNA libraries were prepared using the Illumina
465 TruSeq Stranded mRNA kit modified for improved performance and multiplexing. Libraries

466 were pooled and sequenced with the Illumina HiSeq 4000 using 101-cycle, pair-end settings to
467 obtain 50 million read sequencing depth per sample.
468
469 **RNA read processing and Quantification.** All samples were processed using an RNA-Seq
470 pipeline implemented in the bcbio-nextgen project (https://bcbio-
471 nextgen.readthedocs.io/en/latest/). Raw reads were examined for quality issues using FastQC
472 (http://www.bioinformatics.babraham.ac.uk/projects/fastqc/) to ensure library generation and
473 sequencing data were suitable for further analysis. Reads were aligned to the hg19 build of
474 the human genome using STAR[41]. Quality of alignments was assessed by checking for evenness
475 of coverage, rRNA content, genomic context of alignments, complexity and other quality checks.
476 Expression quantification was performed with Salmon[42] to identify transcript-level abundance
477 estimates and then collapsed down to the gene-level using the R Bioconductor package
478 tximport[43]. Principal components analysis (PCA) and hierarchical clustering methods validated
479 clustering of samples by cell line and group. Differential expression was performed at the gene
480 level using the R Bioconductor package DESeq2[44]. Differentially expressed genes were
481 identified using the Wald test and significant genes were obtained using an FDR threshold of
482 0.05. GSEA[45] was carried out on the full expression data matrix using the gene sets collection
483 from Kyoto Encyclopedia of Genes and Genomes (KEGG) to assess the enrichment of the
484 "adaptation to nutrient deprivation" signature. A pairwise GSEA was performed by creating
485 ranked lists of genes using the difference of class means to calculate fold change for log scale
486 data between the Adapted and Non-Adapted PDA clones (Supplementary Fig. 3) and P values
487 were obtained from permuting the gene set (1000 permutations).
488

489 **ATAC-Seq.** Cells were seeded overnight at 700,000 per 10 cm plate, washed once with PBS,
490 and incubated in L-L medium for 24 h. The assay[46] was performed on 10^6 cells per condition.
491 Cells were washed twice in ice-cold PBS and resuspended in 50 μl ice-cold ATAC lysis buffer
492 (10 mM Tris.Cl, pH 7.4, 10 mM NaCl, 3 mM $MgCl_2$, 0.1% (v/v) Igepal CA-630), and
493 centrifuged at 500 g at 4°C to isolate nuclear pellets that were treated in 50 μL reactions with
494 Nextera Tn5 Transposase (Illumina, FC-121-1030) for 30 min at 37°C. Column-purified DNA
495 (QIAGEN) was stored at 20°C or amplified immediately in 50 μl reactions with high-fidelity 2X
496 PCR Master Mix (New England Biolabs) using a common forward primer and different reverse
497 primers with unique barcodes for each sample. From the reaction mix, 45 μl was kept on ice after
498 5 cycles of PCR, while 5 μl was amplified by qPCR for 20 additional cycles; the remaining 45 μl
499 was then amplified for the 5-7 cycles required to achieve 1/3 of the maximum qPCR
500 fluorescence intensity. Amplified DNA was purified over columns and primer dimers (<100 bp)
501 were removed using AMPure beads (Beckman Coulter). Size distribution of the amplified DNA
502 was analyzed using High-sensitivity Qubit dsDNA Assay Kit (ThermoFisher). High throughout
503 sequencing was performed by Novogene Corporation, Inc. (Sacramento, CA). Computational
504 analysis was performed as described previously[47].
505
506 **Metabolite tracing, extraction and quantification.** For stable isotope tracing experiments, cells
507 were incubated for 24 h in L-L or H-H medium supplemented with either 0.8mM ^{15}N-
508 ammonium chloride (99% enrichment, NLM-467-1) or 0.4mM ^{15}N-leucine (98% enrichment,
509 NLM-142-0.5) purchased from Cambridge Isotope Laboratories. Cells were then rinsed in ice-
510 cold PBS and metabolites extracted with ice-cold 80% methanol, vortexed for 10min at 4°C, and
511 centrifuged at top speed (10min, 10,000 x g, 4°C). Supernatants were transferred to fresh

512 Eppendorf tubes and dried using a SpeedVac. Dried extracts were suspended in 100 μl water and
513 centrifuged at top speed for 10 min, and the supernatant was analyzed using LC-MS. For Figures
514 2a, 3c and e, and Supplementary Figure 4a, data analysis and natural abundance correction of the
515 stable isotope labeling data were performed as previously described[48]. For Figure 3f and
516 Supplementary Figure 7, data were acquired using a hydrophilic interaction liquid
517 chromatography (HILIC)-positive ion mode mass spectrometry (MS) method operated on
518 Nexera X2 UHPLC (Shimadzu Scientific Instruments, Marlborough, MA) coupled to a Q
519 Exactive orbitrap mass spectrometer (Thermo Fisher Scientific, Waltham, MA) as described
520 previously[49], with full scan high resolution MS data collected over 70–800 m/z. For global
521 steady-state metabolite profiling, data were analyzed using MetaboAnalyst 4.0[50], median-
522 normalized, log-transformed, mean-centered and divided by the S.D. of each variable.
523
524 **Animal work.** All mouse studies and procedures were approved by the Animal Care and Use
525 Committee at Boston Children's Hospital. For orthotopic xenografts, 750,000 cells suspended in
526 25 μl 33% Matrigel (Corning, 356231) in Hank's Balanced Salt Solution (HBSS) were injected
527 into the pancreata of male B6.129S7-Rag^{1tm1Mom}/J mice termed Rag1$^{-/-}$ mice (Jackson
528 Laboratory #002216). *In vivo* ultrasound imaging (Vevo 2100, MS550D Scanhead) was
529 performed on mice to detect and quantify tumor growth at the Small Animal Imaging Lab
530 (SAIL) at Boston Children's Hospital. Following experimental endpoint euthanasia, tumors
531 were collected, their dimensions (**a**, **b** and **c**) were measured with a caliper and tumor volume
532 was estimated according to the ellipsoid formula[51]: $4/3 \times \pi \times (a/2 \times b/2 \times c/2)$. Tumor tissue was
533 then either immediately frozen in liquid nitrogen, or fixed in formalin for later processing.
534

535 **Immunohistochemistry and analysis of human samples.** Formalin-fixed paraffin-embedded
536 PDA tissue microarrays (TMAs) with 2–3 cores per case, were sectioned and immunostained
537 with GS antibody (abcam, ab-73593), according to the manufacturer's protocol. A pathologist
538 scored, in a blinded fashion, the intensity of staining on a scale of 0–3 that represented none (0),
539 weak (1), moderate (2), or strong (3) based on the PDA cell staining. Scores for each tumor core
540 were estimated using the following formula: H-score = 0 x (% area of tumor with no staining) +
541 1 x (% tumor area with weak staining) + 2 x (% tumor area with moderate staining) + 3 x (%
542 tumor area with strong staining), where 300 would be the highest score. TMAs were derived
543 from 127 patients with surgically resected PDA from Massachusetts General Hospital. Informed
544 patient consent was waived by the Institutional Review Board or IRB (Protocol Number
545 2009P001838), as the TMAs were generated from discarded material following clinical
546 diagnosis. For analyses of human data, the following variables were from electronic medical
547 records: age, sex, pN and pT stage based on the American Joint Committee on Cancer 8th
548 edition, tumor size, location and grade of differentiation, and presence of lymphovascular and
549 perineural invasion. Survival analyses were performed using overall survival (OS) as the
550 outcome of interest, defined as the time between surgical resection and death from any cause or
551 date of last clinical contact. Survival outcomes were compared based on tertiles of GS staining
552 intensity as assessed by H-scores using the Kaplan-Meier method. Tertile thresholds were 115
553 and 150 H-score units. As secondary analyses, GS intensity was evaluated for its association
554 with baseline clinicopathological characteristics at the time of surgery using the Kruskal-Wallis
555 test. Statistical significance was set at $P < 0.05$. Data analysis was performed using SAS 9.4
556 (version 9.4, SAS Institute, Cary, NC)."
557

558 **Statistical Analysis**

559 Data were presented as mean ± S.D. or ± S.E.M., unless otherwise indicated. When comparing
560 two groups, a two-tailed non-paired Student's t-test was conducted. For three or more groups,
561 one-way ANOVA was conducted except for proliferation curves, where two-way ANOVA was
562 conducted. ANOVA was followed by post hoc Tukey's multiple-comparison test. $p < 0.05$ was
563 considered statistically significant.

564

565 **Acknowledgements**

566 We thank members of the Kalaany lab and the Division of Endocrinology for helpful
567 comments and discussions. This work was supported by the American Cancer Society
568 Research Scholar Grant (RSG-17-070-01-TBG) to N.Y.K. and funds from Boston Children's
569 Hospital. N.Y.K. is also supported by NIH/NCI Grant R01 CA211944. P-Y.T. was partly
570 funded by Top University Strategic Alliance (TUSA) fellowship from Taiwan. Work by M.M.
571 was supported by Harvard Catalyst, The Harvard Clinical and Translational Science Center
572 (NIH award #UL1 RR 025758) and computations were run on the Orchestra cluster supported
573 by HMS Research Computing Group.

574

575 **Author Contributions**

576 N.Y.K. conceived, designed and supervised the study. P-Y.T. performed the experiments with
577 help from lab members and collaborators. M-S.L. performed biochemical assays for GS
578 stabilization and growth assays for stable GS knockdown with help from I.N. who also assisted
579 in macropinocytosis quantification and western blotting. A.A. assisted P-Y.T. with tumor cell
580 injection into mice. M.M. analyzed RNA-Seq data for PCA and helped P-Y.T. in pathway

581 analyses. R.A.M. supervised the ATAC-Seq experiment and analyses, contributing to the
582 interpretation of the results. U.J. performed the ATAC-Seq assay and analyzed the ATAC-Seq
583 and RNA-Seq data with help from S.M. C.A.L. performed metabolite quantification and tracing
584 analyses (Figs 2a and 3c,d and Supplementary Fig. 4). D.S.H., with supervision from C.B.C.,
585 performed metabolite quantification and tracing analyses (Fig. 3f and Supplementary Fig. 7).
586 F.R.R. assisted with mouse ultrasound imaging. M.M.-K. provided TMAs and pathological
587 assessment and scoring for immunostained human pancreatic tissue. T.H. and K.C.H. helped
588 retrieve patient data. P.D. performed the statistical analyses on human data with consultation
589 from V.M.-O. who contributed to the discussion of the results. N.Y.K. and P.-Y.T. wrote the
590 manuscript with feedback from all authors.
591
592 **Supplementary information**
593 Supplementary Figures 1-11 accompany this manuscript.
594
595 **Data availability**
596 The RNA-Seq and ATAC-Seq data have been deposited in NCBI's Gene Expression Omnibus
597 and will be accessible through GEO Series accession number GSE144833.
598
599 **Competing interests**
600 The authors declare no competing financial interests.
601
602
603

604 **References**

605 1. Siegel, R.L., Miller, K.D. & Jemal, A. Cancer statistics, 2019. *CA Cancer J Clin* **69**, 7-34
606 (2019).
607 2. Rahib, L. *et al.* Projecting cancer incidence and deaths to 2030: the unexpected burden of
608 thyroid, liver, and pancreas cancers in the United States. *Cancer Res* **74**, 2913-2921
609 (2014).
610 3. Perera, R.M. & Bardeesy, N. Pancreatic Cancer Metabolism: Breaking It Down to Build
611 It Back Up. *Cancer Discov* **5**, 1247-1261 (2015).
612 4. Ying, H. *et al.* Genetics and biology of pancreatic ductal adenocarcinoma. *Genes Dev* **30**,
613 355-385 (2016).
614 5. Yang, S. *et al.* Pancreatic cancers require autophagy for tumor growth. *Genes Dev* **25**,
615 717-729 (2011).
616 6. Commisso, C. *et al.* Macropinocytosis of protein is an amino acid supply route in Ras-
617 transformed cells. *Nature* **497**, 633-637 (2013).
618 7. Kamphorst, J.J. *et al.* Human pancreatic cancer tumors are nutrient poor and tumor cells
619 actively scavenge extracellular protein. *Cancer Res* **75**, 544-553 (2015).
620 8. Ying, H. *et al.* Oncogenic Kras maintains pancreatic tumors through regulation of
621 anabolic glucose metabolism. *Cell* **149**, 656-670 (2012).
622 9. Son, J. *et al.* Glutamine supports pancreatic cancer growth through a KRAS-regulated
623 metabolic pathway. *Nature* **496**, 101-105 (2013).
624 10. Muir, A. & Vander Heiden, M.G. The nutrient environment affects therapy. *Science* **360**,
625 962-963 (2018).
626 11. Davidson, S.M. *et al.* Environment Impacts the Metabolic Dependencies of Ras-Driven
627 Non-Small Cell Lung Cancer. *Cell Metab* **23**, 517-528 (2016).
628 12. Hensley, C.T. *et al.* Metabolic Heterogeneity in Human Lung Tumors. *Cell* **164**, 681-694
629 (2016).
630 13. Maher, E.A. *et al.* Metabolism of [U-13 C]glucose in human brain tumors in vivo. *NMR*
631 *Biomed* **25**, 1234-1244 (2012).
632 14. Marin-Valencia, I. *et al.* Analysis of tumor metabolism reveals mitochondrial glucose
633 oxidation in genetically diverse human glioblastomas in the mouse brain in vivo. *Cell*
634 *Metab* **15**, 827-837 (2012).
635 15. Sullivan, M.R. *et al.* Quantification of microenvironmental metabolites in murine cancers
636 reveals determinants of tumor nutrient availability. *Elife* **8** (2019).
637 16. Cantor, J.R. *et al.* Physiologic Medium Rewires Cellular Metabolism and Reveals Uric
638 Acid as an Endogenous Inhibitor of UMP Synthase. *Cell* **169**, 258-272 e217 (2017).
639 17. Vande Voorde, J. *et al.* Improving the metabolic fidelity of cancer models with a
640 physiological cell culture medium. *Sci Adv* **5**, eaau7314 (2019).
641 18. Pan, M. *et al.* Regional glutamine deficiency in tumours promotes dedifferentiation
642 through inhibition of histone demethylation. *Nat Cell Biol* **18**, 1090-1101 (2016).
643 19. Lee, S.W. *et al.* EGFR-Pak Signaling Selectively Regulates Glutamine Deprivation-
644 Induced Macropinocytosis. *Dev Cell* (2019).
645 20. Psychogios, N. *et al.* The human serum metabolome. *PLoS One* **6**, e16957 (2011).
646 21. Altman, B.J., Stine, Z.E. & Dang, C.V. From Krebs to clinic: glutamine metabolism to
647 cancer therapy. *Nat Rev Cancer* **16**, 749 (2016).

648 22. Gebregiworgis, T. *et al.* Glucose Limitation Alters Glutamine Metabolism in MUC1-
649 Overexpressing Pancreatic Cancer Cells. *J Proteome Res* **16**, 3536-3546 (2017).
650 23. Tan, H.W.S., Sim, A.Y.L. & Long, Y.C. Glutamine metabolism regulates autophagy-
651 dependent mTORC1 reactivation during amino acid starvation. *Nat Commun* **8**, 338
652 (2017).
653 24. Yan, L., Raj, P., Yao, W. & Ying, H. Glucose Metabolism in Pancreatic Cancer. *Cancers*
654 *(Basel)* **11** (2019).
655 25. Ben-Sahra, I., Howell, J.J., Asara, J.M. & Manning, B.D. Stimulation of de novo
656 pyrimidine synthesis by growth signaling through mTOR and S6K1. *Science* **339**, 1323-
657 1328 (2013).
658 26. Harrington, L.S. *et al.* The TSC1-2 tumor suppressor controls insulin-PI3K signaling via
659 regulation of IRS proteins. *J Cell Biol* **166**, 213-223 (2004).
660 27. Hsu, P.P. *et al.* The mTOR-regulated phosphoproteome reveals a mechanism of
661 mTORC1-mediated inhibition of growth factor signaling. *Science* **332**, 1317-1322
662 (2011).
663 28. Shah, O.J., Wang, Z. & Hunter, T. Inappropriate activation of the TSC/Rheb/mTOR/S6K
664 cassette induces IRS1/2 depletion, insulin resistance, and cell survival deficiencies. *Curr*
665 *Biol* **14**, 1650-1656 (2004).
666 29. Nguyen, T.V. *et al.* Glutamine Triggers Acetylation-Dependent Degradation of
667 Glutamine Synthetase via the Thalidomide Receptor Cereblon. *Mol Cell* **61**, 809-820
668 (2016).
669 30. Nguyen, T.V. *et al.* p97/VCP promotes degradation of CRBN substrate glutamine
670 synthetase and neosubstrates. *Proc Natl Acad Sci U S A* **114**, 3565-3571 (2017).
671 31. Allen, P.J. *et al.* Multi-institutional Validation Study of the American Joint Commission
672 on Cancer (8th Edition) Changes for T and N Staging in Patients With Pancreatic
673 Adenocarcinoma. *Ann Surg* **265**, 185-191 (2017).
674 32. Bott, A.J. *et al.* Glutamine Anabolism Plays a Critical Role in Pancreatic Cancer by
675 Coupling Carbon and Nitrogen Metabolism. *Cell Rep* **29**, 1287-1298 e1286 (2019).
676 33. Yuneva, M.O. *et al.* The metabolic profile of tumors depends on both the responsible
677 genetic lesion and tissue type. *Cell Metab* **15**, 157-170 (2012).
678 34. Tardito, S. *et al.* Glutamine synthetase activity fuels nucleotide biosynthesis and supports
679 growth of glutamine-restricted glioblastoma. *Nat Cell Biol* **17**, 1556-1568 (2015).
680 35. Issaq, S.H., Mendoza, A., Fox, S.D. & Helman, L.J. Glutamine synthetase is necessary
681 for sarcoma adaptation to glutamine deprivation and tumor growth. *Oncogenesis* **8**, 20
682 (2019).
683 36. Biancur, D.E. *et al.* Compensatory metabolic networks in pancreatic cancers upon
684 perturbation of glutamine metabolism. *Nat Commun* **8**, 15965 (2017).
685 37. Muir, A. *et al.* Environmental cystine drives glutamine anaplerosis and sensitizes cancer
686 cells to glutaminase inhibition. *Elife* **6** (2017).
687 38. Zhao, J., Zhai, B., Gygi, S.P. & Goldberg, A.L. mTOR inhibition activates overall protein
688 degradation by the ubiquitin proteasome system as well as by autophagy. *Proc Natl Acad*
689 *Sci U S A* **112**, 15790-15797 (2015).
690 39. Commisso, C., Flinn, R.J. & Bar-Sagi, D. Determining the macropinocytic index of cells
691 through a quantitative image-based assay. *Nat Protoc* **9**, 182-192 (2014).
692 40. Bookout, A.L. & Mangelsdorf, D.J. Quantitative real-time PCR protocol for analysis of
693 nuclear receptor signaling pathways. *Nucl Recept Signal* **1**, e012 (2003).

694 41. Dobin, A. *et al.* STAR: ultrafast universal RNA-seq aligner. *Bioinformatics* **29**, 15-21
695 (2013).
696 42. Patro, R., Duggal, G., Love, M.I., Irizarry, R.A. & Kingsford, C. Salmon provides fast
697 and bias-aware quantification of transcript expression. *Nat Methods* **14**, 417-419 (2017).
698 43. Soneson, C., Love, M.I. & Robinson, M.D. Differential analyses for RNA-seq: transcript-
699 level estimates improve gene-level inferences. *F1000Res* **4**, 1521 (2015).
700 44. Love, M.I., Huber, W. & Anders, S. Moderated estimation of fold change and dispersion
701 for RNA-seq data with DESeq2. *Genome Biol* **15**, 550 (2014).
702 45. Subramanian, A. *et al.* Gene set enrichment analysis: a knowledge-based approach for
703 interpreting genome-wide expression profiles. *Proc Natl Acad Sci U S A* **102**, 15545-
704 15550 (2005).
705 46. Buenrostro, J.D., Wu, B., Chang, H.Y. & Greenleaf, W.J. ATAC-seq: A Method for
706 Assaying Chromatin Accessibility Genome-Wide. *Curr Protoc Mol Biol* **109**, 21 29 21-
707 29 (2015).
708 47. Jadhav, U. *et al.* Dynamic Reorganization of Chromatin Accessibility Signatures during
709 Dedifferentiation of Secretory Precursors into Lgr5+ Intestinal Stem Cells. *Cell Stem Cell*
710 **21**, 65-77 e65 (2017).
711 48. Kanarek, N. *et al.* Histidine catabolism is a major determinant of methotrexate sensitivity.
712 *Nature* **559**, 632-636 (2018).
713 49. Mascanfroni, I.D. *et al.* Metabolic control of type 1 regulatory T cell differentiation by
714 AHR and HIF1-alpha. *Nature medicine* **21**, 638-646 (2015).
715 50. Chong, J., Wishart, D.S. & Xia, J. Using MetaboAnalyst 4.0 for Comprehensive and
716 Integrative Metabolomics Data Analysis. *Curr Protoc Bioinformatics* **68**, e86 (2019).
717 51. Wapnir, I.L., Wartenberg, D.E. & Greco, R.S. Three dimensional staging of breast
718 cancer. *Breast Cancer Res Treat* **41**, 15-19 (1996).
719

720

721

722

723

724

725

726

727

728

729

730 **Figure Legends**

731 **Figure 1. PDA cells adapted to nutrient deprivation exhibit enhanced growth *in vitro* and *in***
732 ***vivo*. a**, Schematic depicting selection of adapted (A) clones (C4-C6) derived from 8988T or
733 SUIT-2 human PDA cells that survived and grew in low glucose-low glutamine (L-L) medium,
734 and control non-adapted (NA) clones (C1-C3) derived from parental cells plated at low dilution
735 in high glucose-high glutamine (H-H) medium. **b**, Proliferation curves of clonal cells described
736 in **a** that were grown in L-L medium for 7 days (n= 5). **c**, Percent cell death in clones described
737 in **a** (n= 5) that were grown in L-L medium for 4 days (SUIT-2) or 5 days (8988T). **d**, Colony
738 formation assay showing number of colonies formed by 8988T or SUIT-2 cells described in **a**
739 that were grown in L-L medium for 10 days or 7 days, respectively (n= 6). **e**, Three-dimensional
740 (3D) growth assay showing area of spheres formed by 8988T or SUIT-2 cells described in **a** that
741 were grown for 10 days or 7 days, respectively, in L-L medium supplemented with 4% matrigel
742 (n= 6). **f**, Volumes of orthotopic xenograft PDA tumors derived from 8988T clones described in
743 **a** that were injected (75 x 10^4 cells) into the pancreas of 4-6 week old $Rag1^{-/-}$ mice and grown for
744 33 days (n=7 for NA-C1; n=6 for NA-C2 and n=7 for A-C4, 5 clones). Data represent the mean
745 ± S.E.M. in **b**, or mean ± S.D. in **c-f**. *$p < 0.05$; **$p < 0.01$; ***$p < 0.001$; ****$p < 0.0001$, two-
746 way ANOVA for **b** and one-way ANOVA for **c-f**, followed by Tukey test.

747

748 **Figure 2. Adapted PDA clones display enhanced *de novo* DNA synthesis and mTORC1**
749 **signaling under nutrient-deprived conditions. a**, Heatmap listing in descending order of
750 statistical significance ($p < 0.05$ by *t* test) metabolites in the purine and pyrimidine synthesis
751 pathways for non-adapted or adapted PDA clones, that were treated for 24 h with L-L medium
752 (n= 4 replicates per clone, except for 8988T C5: n= 3). Red indicates higher level and blue lower

753 level, relative to the median for each metabolite across all groups. **b**, Relative incorporation of
754 radiolabeled U-^{14}C-aspartate into DNA synthesis in non-adapted (NA-C) and adapted (A-C)
755 SUIT-2 clones treated with either L-L or H-H medium for 40 h. Data are presented as relative
756 fold change normalized to NA-C1 under L-L conditions and represent the mean ± S.D. (n= 3
757 replicates per clone). *$p < 0.05$; **$p < 0.01$, one-way ANOVA followed by Tukey test. **c**,
758 Immunoblots of pT389-S6K, pS65-4EBP1, pS1859-CAD and total S6K, 4EBP1, CAD in 8988T
759 or SUIT-2 clones treated with H-H or L-L medium for 24 h. β-actin was used as a loading
760 control.
761
762 **Figure 3. Adapted PDA cells induce GS and have enhanced incorporation of nitrogen from**
763 **amino acids into glutamine and nucleotide synthesis. a,** Schematic illustrating glutamate
764 synthesis from α-ketoglutarate (α-KG) and ammonia by glutamate dehydrogenase (GDH) and
765 glutamine synthesis from glutamate and ammonia by glutamine synthetase (GS). In red, are
766 ammonia nitrogens incorporating into glutamate and then glutamine. **b**, Immunoblots of GS (low
767 or high exposures) and GDH in 8988T or SUIT-2 clones treated with H-H or L-L medium for 24
768 h. β-actin was used as a loading control. **c**, Fractional labeling of ^{15}N-glutamate and glutamine in
769 SUIT-2 cells treated for 24 h with H-H or L-L medium supplemented with 0.8mM ^{15}N-
770 ammonium chloride. Data are corrected for natural abundance and represent the average of 4
771 replicates per clone per condition ± S.D. *$p < 0.05$; ****$p < 0.0001$, one-way ANOVA followed
772 by Tukey test. **d**, Schematic illustrating the incorporation of leucine nitrogen (red) into glutamate
773 and then aspartate via transamination reactions catalyzed by branched chain amino acid
774 transaminase BCAT and aspartate transaminase GOT. Glutamate is used to synthesize glutamine
775 via GS and aspartate nitrogen incorporates into newly synthesized nucleotides. **e**, Heatmap

776 listing in descending order of statistical significance ($p < 0.05$ by t test) amino acids in non-
777 adapted or adapted PDA clones that were treated for 24 h with L-L medium (n= 4 per clone per
778 condition, except for 8988T C5: n= 3). Red indicates higher level and blue lower level, relative
779 to the median for each metabolite across all groups. **f**, Fractional labeling of metabolites in
780 glutamine and nucleotide synthesis pathways in cells described in **b** grown in media
781 supplemented with 0.4mM ^{15}N-leucine for 24 h. Data represent the average of 4 replicates per
782 clone per condition ± S.D. *$p < 0.05$; ****$p < 0.0001$, one-way ANOVA followed by Tukey
783 test.
784
785 **Figure 4. PDA adaptation to nutrient deprivation is reversible and associated with changes**
786 **in open chromatin. a,** Schematic depicting the adaptation reversal process where adapted PDA
787 clones are grown in nutrient replete (H-H) conditions for at least 4 passages, prior to treatment
788 with H-H or L-L medium for 24 h. **b**, Immunoblots of pT389-S6K (low and high exposures),
789 pS65-4EBP1, pS1859-CAD and total S6K, 4EBP1, CAD and GS in SUIT (C5) or 8988T (C4)
790 clones that were reverse-adapted over 4 passages and then treated with H-H or L-L medium for
791 24 h. β-actin was used as a loading control. **c**, Proliferation curves of SUIT-2 or 8988T cells that
792 are either non-adapted (NA), adapted (A) or reverse adapted (RA) for 18 passages (SUIT-2) or
793 30 passages (8988T) and grown under L-L conditions for 7 days (n= 6). **d**, Percent cell death in
794 clones described in **c** that were grown under L-L medium for 5 days (n= 6). Data represent the
795 mean ± S.E.M. in **c**, and mean ± S.D. in **d**. **$p < 0.01$; ***$p < 0.001$; ****$p < 0.0001$, two-way
796 ANOVA for **c** and one-way ANOVA for **d**, followed by Tukey test. In **c**, stars indicate statistical
797 significance for A vs NA; A vs RA; RA vs NA; ns indicates non-significance for A vs RA (day
798 3) and RA vs NA (day 7) in 8988T cells. **e**. Relative mRNA levels of 1,842 genes upregulated

799 (>3-fold, q <0.05) in both SUIT-2 and 8988T adapted clones, compared to non-adapted clones;
800 mRNA levels of the corresponding genes in reverse-adapted (RA) clones are shown alongside.
801 Differentially expressed genes were identified by unsupervised k-means clustering. Red, high
802 expression; blue, reduced expression relative to mean expression levels for each gene across all
803 groups (n= 3 clones per group). **f**, ATAC-seq data showing significant (>2-fold, q <0.05)
804 changes in chromatin access at enhancers (located >500 bp from transcription start sites) in each
805 of 2 independent non-adapted (NA), adapted (A), and reverse-adapted (RA) 8988T or SUIT-2
806 clones. **g**, Correlation of changes in gene expression and nearby (<25 kb) chromatin accessibility
807 for the 1,842 genes induced upon adaptation to nutrient deprivation in both SUIT-2 and 8988T
808 cells. Each dot represents a gene, and those linked to 3,807 enhancers with altered chromatin
809 access in both cell lines are marked in purple. More gene-linked enhancers (<25 kb) show gains
810 than show losses in accessibility.
811
812 **Figure 5. mTORC1 stabilizes GS protein levels under glutamine deprivation.**
813 **a**, Immunoblots of GS (low and high exposures), pT389-S6K and total S6K in SUIT-2 or 8988T
814 adapted clones (C4-C6) that were treated with vehicle control (DMSO) or Torin 1 (40 nM) in L-
815 L medium for 24 h. **b**, Immunoblots of GS, pS65-4EBP1, pT389-S6K, total 4EBP1 or S6K in
816 cells from **a** that were treated under L-L medium with control DMSO or Torin 1 (200 nM) for a
817 total of 8 h, in the absence or presence of cycloheximide (CHX, 20 μg ml^{-1}) for the indicated
818 times. **c**, GS protein levels in non-adapted and adapted SUIT-2 or 8988T clones treated in L-L
819 medium with MG-132 (10μM) for the indicated times. **d**, GS protein levels in SUIT-2 or 8988T
820 adapted clones treated in L-L medium with either Torin 1 (200 nM) or MG-132 (10μM) alone, or
821 in combination for 12 h (C4) or 8 h (C5, C6). **e**, Co-immunoprecipitation (IP) blots showing the

822 ubiquitination status of GS in SUIT-2 or 8988T adapted clones treated in L-L medium, with
823 either Torin 1 (200 nM) or MG-132 (10μM) alone, or in combination for 8 h. Input refers to
824 immunoblots of total GS, pT389-S6K and total S6K levels in whole cell lysates. In **a-e**, β-actin
825 or GAPDH were used as loading controls.
826
827 **Figure 6. GS is required for the adaptation-induced growth fitness of PDA cells under**
828 **nutrient deprivation. a,** Proliferation curves of adapted 8988T cells transfected with
829 Doxycycline (Dox)-inducible shScrambled control or shGS hairpins 1 and 2, grown in L-L
830 medium for 7 days in the absence or presence of 1 μg ml^{-1} Dox (n= 8). **b**, Percent cell death in
831 cells described in **a** (n= 8) that were grown in L-L medium for 7 days. **c**, Colony formation assay
832 for cells in **a** that were grown for 10 days, under L-L conditions (n= 6). **d**, Weights of orthotopic
833 xenograft PDA tumors derived from 8988T adapted cells (C4) stably expressing Dox-inducible
834 hairpins described in **a** that were injected (75 x 10^4 cells) into the pancreas of 4-6 week old $Rag1^{-}$
835 $^{/-}$ mice. Dox was supplemented in the drinking water (2 mg ml^{-1}) 5 days post-injection of cells,
836 and tumors were harvested 33 days later (n=5 shScr -Dox; n= 7 shScr + Dox; n= 8 shGS#1; n= 7
837 shGS#2). Data represent the mean ± S.E.M. in **a**, and mean ± S.D. in **b-d**. $^{**}p < 0.01$; $^{***}p <$
838 0.001; $^{****}p < 0.0001$, two-way ANOVA for **a**, one-way ANOVA for **b-d**, followed by Tukey
839 test. **e**, Immunoblots of GS in cells used for xenografts in **d** showing decreased protein levels, 48
840 h following treatment with Dox (1 μg ml^{-1}) for inducible knockdown . β-actin was used as a
841 loading control. **f**, Model illustrating a role for GS stabilization in PDA cell adaptation to nutrient
842 deprivation, which leads to enhanced growth fitness. The sketch was created using
843 Biorender.com.
844

845 **Supplementary Figure Legends**

846 **Supplementary Figure 1. Adaptation to nutrient deprivation enhances PDA cell growth**
847 **potential.**

848 **A**, Proliferation curves of adapted 8988T or SUIT-2 PDA clones (A-C4, -C5, -C6) and control
849 non-adapted (NA-C1, -C2, -C3) clones that were grown in H-H medium for 7 days (n= 6). **B**,
850 Percent cell death in clones described in **a** that were grown in H-H medium for 5 days (n= 6). **C**,
851 Colony formation assay showing number of colonies formed by cells in **a** that were grown for 10
852 days (8988T) or 7 days (SUIT-2) under H-H conditions (n= 6). **D-f**, 3D growth assay showing
853 number (**d**, **e**) or area (**f**) of spheres formed by cells in **a** that were grown for 10 days or 7 days,
854 respectively, in L-L (**d**) or H-H (**e, f**) medium supplemented with 4% matrigel (n= 6). **G,**
855 Representative images of mice bearing orthotopic transplants of adapted or non-adapted PDA
856 clones. Boxed areas are enlarged on the right, demonstrating the presence of a large pancreatic
857 tumor derived from the adapted cells and absence of tumors on the pancreas that was previously
858 injected with non-adapted cells. Data represent the mean ± S.E.M. in **a**, and mean ± S.D. in **b-f**.
859 *$p < 0.05$; **$p < 0.01$; ***$p < 0.001$; ****$p < 0.0001$, two-way ANOVA for **a** and one-way
860 ANOVA for **b-f**, followed by Tukey test.

861

862 **Supplementary Figure 2. Autophagy and macropinocytosis are not further induced in PDA**
863 **cells upon adaptation to nutrient deprivation. A and b,** Immunoblots of the autophagy marker
864 LC3B-II in SUIT-2 (**a**) or 8988T (**b**) non-adapted (NA) or adapted (A) clones treated under L-L
865 medium, with the autophagy inhibitor chloroquine (CQ, 10 μM) for 2, 6 or 24 h. Blots
866 demonstrate similar or decreased autophagic flux in adapted compared to non-adapted cells. **C**,
867 Representative images for macropinocytic uptake of TMR-dextran by non-adapted and adapted

868 8988T and SUIT-2 cells in the presence or absence of the inhibitor EIPA (top) with
869 quantification of macropinocytic area per cell (bottom). Scale bar, 25 μm. Data represent the
870 mean ± S.D. for n= 2 independent experiments with approximately 165 cells (8988T) or 285
871 cells (SUIT-2) scored per experiment. ****$p < 0.0001$, one-way ANOVA followed by Tukey
872 test.
873
874 **Supplementary Figure 3. Adaptation to nutrient deprivation minimizes transcriptional**
875 **variance between PDA cell lines. A,** Principal Component Analysis (PCA) of the 500 most
876 variable genes in adapted and non-adapted PDA clones; n = 3 clones per group. Samples
877 segregate based on cell line or PC1, which explains 83% of the variance. Segregation is
878 minimized upon adaptation to nutrient deprivation (PC2, 8% variance). **B**, Heatmaps (left) of
879 genes enriched in metabolic pathways in adapted compared to non-adapted SUIT-2 or 8988T
880 clones (n = 3 per group), with corresponding GSEA plots (right). Red indicates higher
881 expression, and blue lower expression, relative to the mean expression level for each metabolite
882 across all groups. NES normalized enrichment scores, FDR false discovery rate, Nom. Nominal.
883
884 **Supplementary Figure 4. Nutrient-deprived adapted PDA cells display metabolite levels**
885 **closer to those under nutrient-replete conditions. a**, Heatmap listing in descending order of
886 statistical significance ($p < 0.05$ by *t* test), amino acids, metabolites in the nucleotide synthesis
887 pathway, and metabolites in the TCA cycle, glycolysis/gluconeogenesis pathways in non-adapted
888 or adapted PDA clones from SUIT-2 or 8988T cells that were treated for 24 h with H-H or L-L
889 medium. Data represent 3 clones per condition with n= 4 replicates per clone). Red indicates
890 higher level and blue lower level, relative to the median for each metabolite across all groups. **B**,

891 List of top 27 metabolic pathways in descending order of statistical significance (-log $p \geq 2.18$;
892 FDR ≤ 10E-10) that are enriched in adapted, compared to non-adapted PDA clones from both
893 cell lines, under L-L medium. In bold are pathways involving metabolites in **a**. FDR, false
894 discovery rate.
895
896 **Supplementary Figure 5. AKT phosphorylation is decreased in adapted PDA clones under**
897 **nutrient deprivation. A,** Immunoblots of pS473-AKT, pT389-AKT and total AKT in non-
898 adapted (NA) and adapted (A) SUIT-2 clones (C1-C6) under H-H and L-L medium. GAPDH
899 was used as loading control.
900
901 **Supplementary Figure 6. Transaminase expression is induced in adapted PDA cells under**
902 **nutrient deprivation. A** and **b,** Relative mRNA levels of GS (**a**), and transaminases BCAT1/2
903 and GOT1/2 (**b**) in adapted (A) or non-adapted (NA) SUIT-2 and 8988T cells treated for 24 h
904 with either H-H or L-L medium. Data represent the mean of 3 clones per condition ± S.D., n = 3
905 replicates per clone. $^{**}p < 0.01$; $^{***}p < 0.001$; $^{****}p < 0.0001$, one-way ANOVA followed by
906 Tukey test. **C**, Levels of BCAT1/2, GOT1/2 proteins in cells described in **a** and **b** under L-L
907 medium. β-actin was used as loading control.
908
909 **Supplementary Figure 7. Branched chain amino acids serve as a source of nitrogen for**
910 **glutamine synthesis in adapted PDA clones. A,** Fractional labeling of metabolites in non-
911 adapted (NA) or adapted (A) 8988T clones (C1-C6) treated with L-L medium supplemented with
912 0.4mM ^{15}N-leucine for 24 h. Data represent the average of 4 replicates per clone per condition ±

913 S.D. *$p < 0.05$; **$p < 0.01$; ***$p < 0.001$; ****$p < 0.0001$, one-way ANOVA followed by
914 Tukey test.
915
916 **Supplementary Figure 8. Reverse adaptation of PDA cells to nutrient deprivation results in**
917 **reversal of enhanced growth and maintenance of the adaptation-induced chromatin**
918 **accessibility changes. a**, **b** Immunoblots of pT389-S6K (low and high exposures), pS65-4EBP1,
919 pS1859-CAD and total S6K, 4EBP1 and GS in adapted SUIT-2 (**a**) or 8988T (**b**) cells that were
920 reverse-adapted over at least 4 passages and then treated with H-H or L-L medium for 24 h.
921 GAPDH or β-actin was used as a loading control. **c**, Proliferation curves of SUIT-2 and 8988T
922 cells that are either non-adapted (NA), adapted (A) or reverse-adapted (RA) for 18 passages
923 (SUIT-2) or 30 passages (8988T) and grown under L-L conditions for 7 days (n= 6). Data
924 represent the mean ± S.E.M. *$p < 0.05$; **$p < 0.01$; ****$p < 0.0001$, two-way ANOVA followed
925 by Tukey test, and indicate significant differences for A vs NA; A vs RA; RA vs NA; ns, non-
926 significant for RA vs NA (day 3, SUIT-2); RA vs NA (day 5 and day 7, 8988T).). **d**, Overlap of
927 enhancers with altered chromatin accessibility in adapted 8988T and SUIT-2 cells identifies
928 3,807 sites changed in both cell lines. **e**, Gains and losses in chromatin accessibility during
929 adaptation (NA, non-adapted; A, adapted) of 8988T and SUIT-2 cells, revealing significant
930 correlation (BETA analysis) with increases and decreases, respectively, in gene expression. **f**,
931 Representative loci showing concordant changes in ATAC-seq and RNA-seq signals at *POLE2*
932 and *RRM2*. Dotted boxes demarcate enhancer elements linked to genes that show gain or loss of
933 chromatin accessibility and concordant changes in gene expression in cells adapted to nutrient
934 deprivation. Reversal of chromatin accessibility changes upon reverse adaptation was infrequent

935 (e.g., *RRM2*); enhancers that gained chromatin accessibility upon adaptation generally remained
936 accessible, despite partial reversal in mRNA expression (e.g. *POLE2* in SUIT-2 cells).
937
938 **Supplementary Figure 9. Protein levels of glutamine synthetase are decreased upon Torin 1**
939 **treatment at a post-translational level. a,** Relative mRNA levels of GS in SUIT-2 and 8988T
940 adapted clones (C4, C5, C6) treated with L-L medium in the absence or presence of Torin 1 (200
941 nM) for 24 h. Data represent the mean ± S.D. (n= 3 replicates per clone per condition). $^{**}p <$
942 0.01; $^{***}p < 0.001$; $^{****}p < 0.0001$, one-way ANOVA followed by Tukey test.
943 **b**, Immunoblots of GS, pT389-S6K and total S6K in cells from **a** that were treated under L-L
944 medium with control DMSO or Torin 1 (200 nM) for a total of 8 h, in the absence or presence of
945 cycloheximide (CHX, 20 $\mu g\ ml^{-1}$) for the indicated times prior to cell lysis. β-actin was used as
946 loading control.
947
948 **Supplementary Figure 10. Inhibition of glutamine synthetase suppresses the growth of**
949 **PDA cells adapted to nutrient deprivation. a**, Fold change in cell number of 8988T or SUIT-2
950 adapted clones, 72 h following treatment with the GS inhibitor (MSO) compared to vehicle
951 (water) control, showing decrease in cell number upon GS inhibition under L-L but not H-H
952 conditions (n= 5 per condition). **b**, Proliferation curves of adapted 8988T cells transfected with
953 control non-targeting siRNA or siGS, that were grown in L-L medium for 4 days (n= 6). **c**,
954 Colony formation assay for cells described in b that were grown for 8 days, under L-L conditions
955 (n= 6). **d**, Immunoblots showing GS levels in cells from **b**, 24h post-transfection of siRNA. **e**,
956 Volumes quantified by ultrasound on day 29, of orthotopic PDA xenograft tumors derived from
957 8988T clonal adapted cells (C4) stably expressing Doxycycline (Dox)-inducible hairpins for GS

958 or control Scrambled hairpin. Cells (750 x 10^3) were injected on day 0 into the pancreas of 4-6
959 week old $Rag1^{-/-}$ mice and Dox was supplemented in the drinking water (2 mg ml^{-1}) on day 5
960 (n=5 shScr -Dox; n= 7 shScr + Dox; n= 8 shGS#1; n= 7 shGS#2). **f**, Representative ultrasound
961 images on day 29 of adapted 8988T orthotopic xenograft tumors described in **e**. Data represent
962 the mean ± S.D. in **a, c-e**, and mean ± S.E.M. in **b**. *$p < 0.05$; **$p < 0.01$; ***$p < 0.001$; ****$p <$
963 0.0001, one-way ANOVA for **a** and **e,** two-way ANOVA for **b**, followed by Tukey test, and
964 Student's t-test for **c**.
965
966 **Supplementary Figure 11. Glutamine synthetase average protein levels do not associate**
967 **with human PDA tumor grade or patient survival. a,** Kruskal-Wallis test for associations
968 between GS level (H-score) and tumor size (pT), lymph node involvement (pN), or grade (tumor
969 differentiation level) at time of resection. Low grade indicates well-differentiated tumors;
970 Intermediate grade, moderately differentiated tumors; High grade, poorly differentiated tumors.
971 **b,** Representative images of human normal pancreatic parenchyma with GS staining in acinar
972 cells (red arrowhead), duct cells (black arrowhead), islets (black arrows) and acinar ductal
973 metaplasia (ADM, circled). Staining in human PDA shows no correlation of GS with tumor
974 grade, as many lower-grade tumors display high GS protein levels and higher-grade tumors
975 display low GS levels. **c**, Kaplan Meier survival curves stratified by GS level, categorized as
976 tertiles. Follow-up period is indicated in months. Median survival is slightly shorter for patients
977 with low GS compared to patients with medium or high GS levels. However, the differences
978 between the survival curves are not statistically significant, based on the Log-Rank test ($P =$
979 0.18). These results are consistent with a multivariate Cox proportional hazard regression model
980 that adjusted for age, sex, and tumor grade.

Figure 1

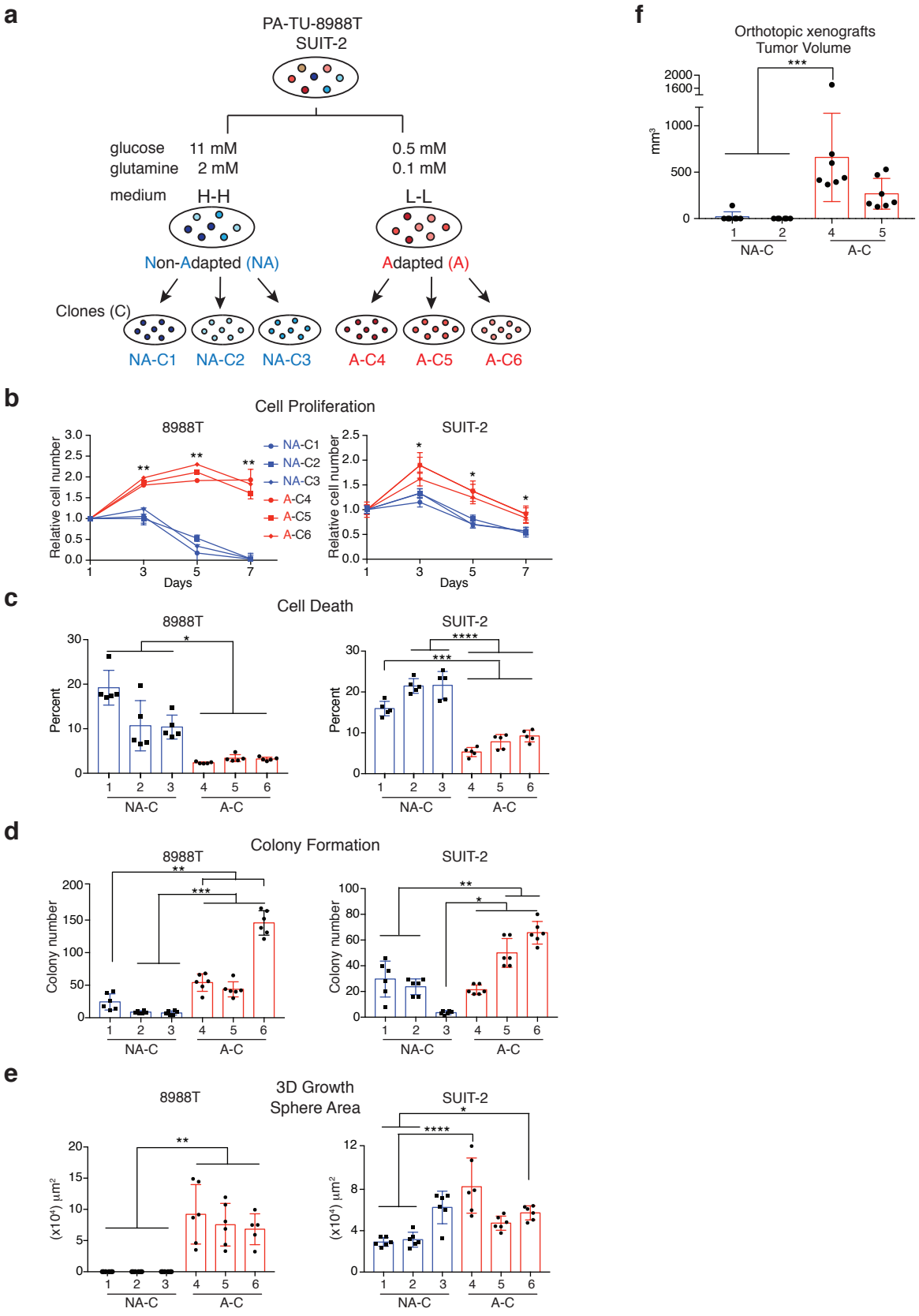
a
PA-TU-8988T
SUIT-2
glucose 11 mM
glutamine 2 mM
0.5 mM
0.1 mM
medium H-H
L-L
Non-Adapted (NA)
Adapted (A)
Clones (C)
NA-C1 NA-C2 NA-C3 A-C4 A-C5 A-C6
b
Cell Proliferation
8988T
SUIT-2
Relative cell number
Days
NA-C1
NA-C2
NA-C3
A-C4
A-C5
A-C6
c
Cell Death
8988T
SUIT-2
Percent
NA-C
A-C
d
Colony Formation
8988T
SUIT-2
Colony number
NA-C
A-C
e
3D Growth
Sphere Area
8988T
SUIT-2
(x10⁴) µm²
NA-C
A-C
f
Orthotopic xenografts
Tumor Volume
mm³
NA-C
A-C

Figure 2

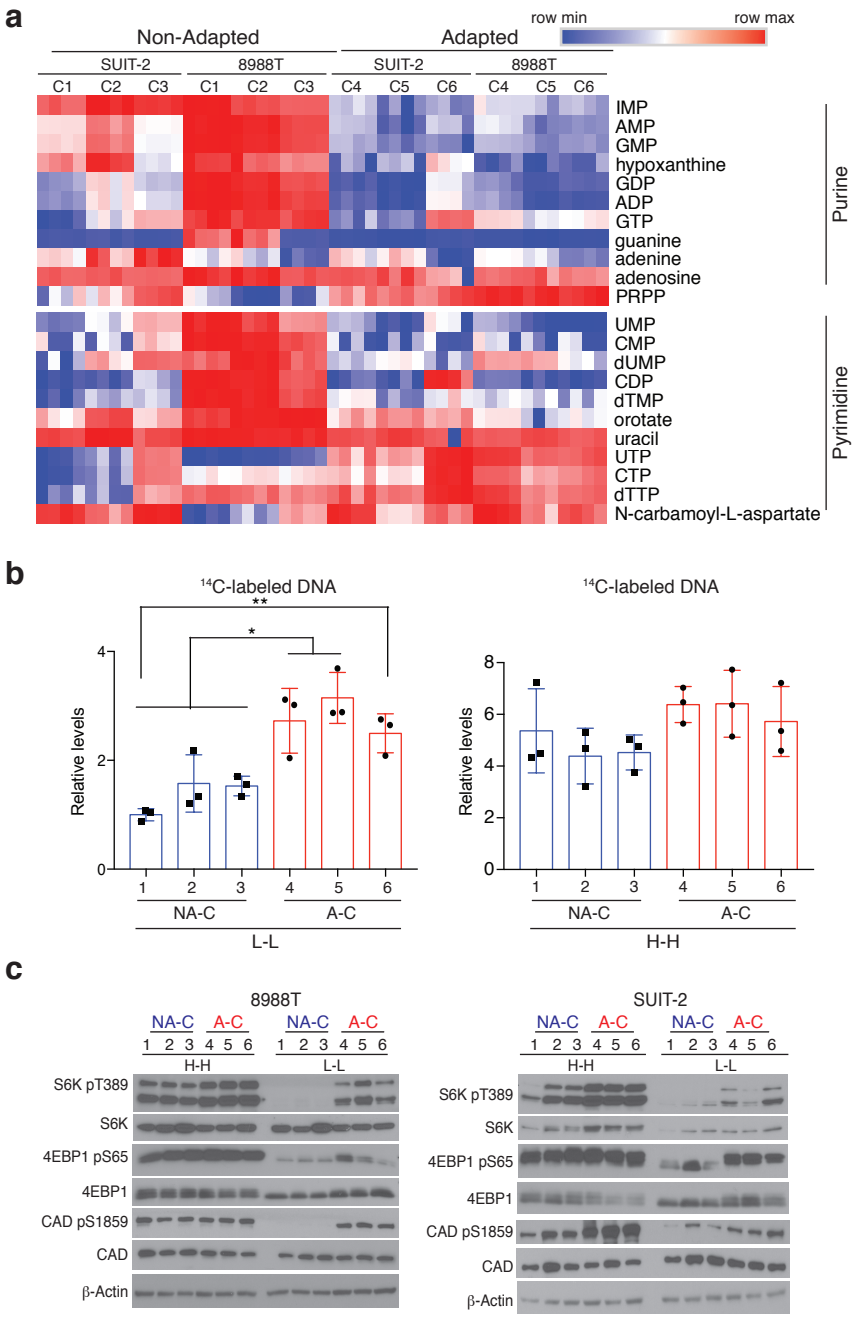
a
Non-Adapted
Adapted
row min
row max
SUIT-2
8988T
SUIT-2
8988T
C1 C2 C3 C1 C2 C3 C4 C5 C6 C4 C5 C6
IMP
AMP
GMP
hypoxanthine
GDP
ADP
GTP
guanine
adenine
adenosine
PRPP
Purine
UMP
CMP
dUMP
CDP
dTMP
orotate
uracil
UTP
CTP
dTTP
N-carbamoyl-L-aspartate
Pyrimidine
b
14C-labeled DNA
Relative levels
NA-C
A-C
L-L
14C-labeled DNA
Relative levels
NA-C
A-C
H-H
c
8988T
NA-C A-C NA-C A-C
1 2 3 4 5 6 1 2 3 4 5 6
H-H
L-L
S6K pT389
S6K
4EBP1 pS65
4EBP1
CAD pS1859
CAD
β-Actin
SUIT-2
NA-C A-C NA-C A-C
1 2 3 4 5 6 1 2 3 4 5 6
H-H
L-L
S6K pT389
S6K
4EBP1 pS65
4EBP1
CAD pS1859
CAD
β-Actin

Figure 3

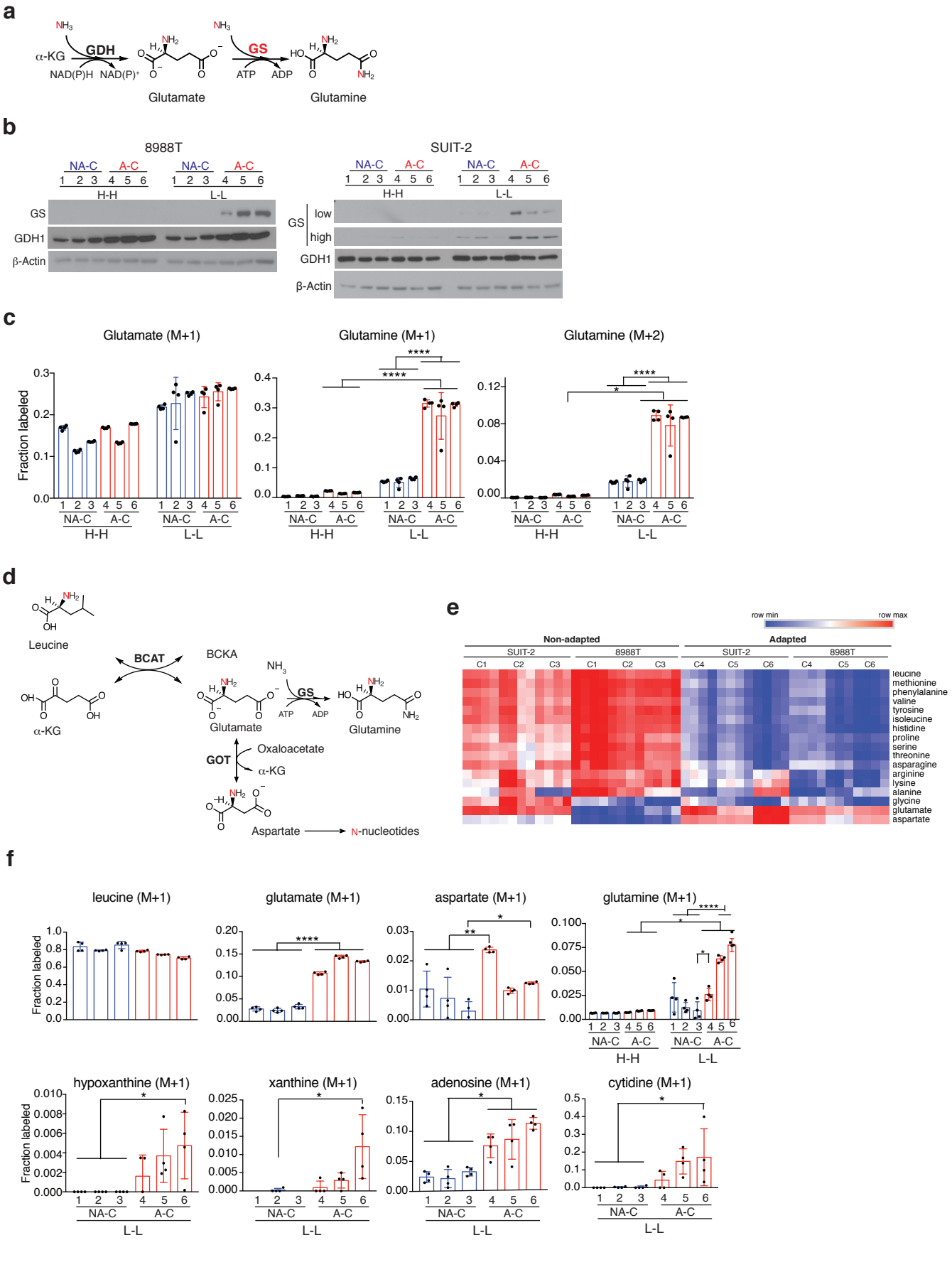

a
α-KG
GDH
NAD(P)H NAD(P)+
Glutamate
GS
ATP ADP
Glutamine
b
8988T
SUIT-2
NA-C A-C
H-H
L-L
GS
GDH1
β-Actin
low
high
c
Glutamate (M+1)
Glutamine (M+1)
Glutamine (M+2)
Fraction labeled
d
Leucine
BCAT
BCKA
α-KG
Glutamate
Glutamine
GOT
Oxaloacetate
Aspartate
N-nucleotides
e
row min
row max
Non-adapted
Adapted
SUIT-2
8988T
C1 C2 C3 C4 C5 C6
leucine
methionine
phenylalanine
valine
tyrosine
isoleucine
histidine
proline
serine
threonine
asparagine
arginine
lysine
alanine
glycine
glutamate
aspartate
f
leucine (M+1)
glutamate (M+1)
aspartate (M+1)
glutamine (M+1)
hypoxanthine (M+1)
xanthine (M+1)
adenosine (M+1)
cytidine (M+1)
Fraction labeled

Figure 4

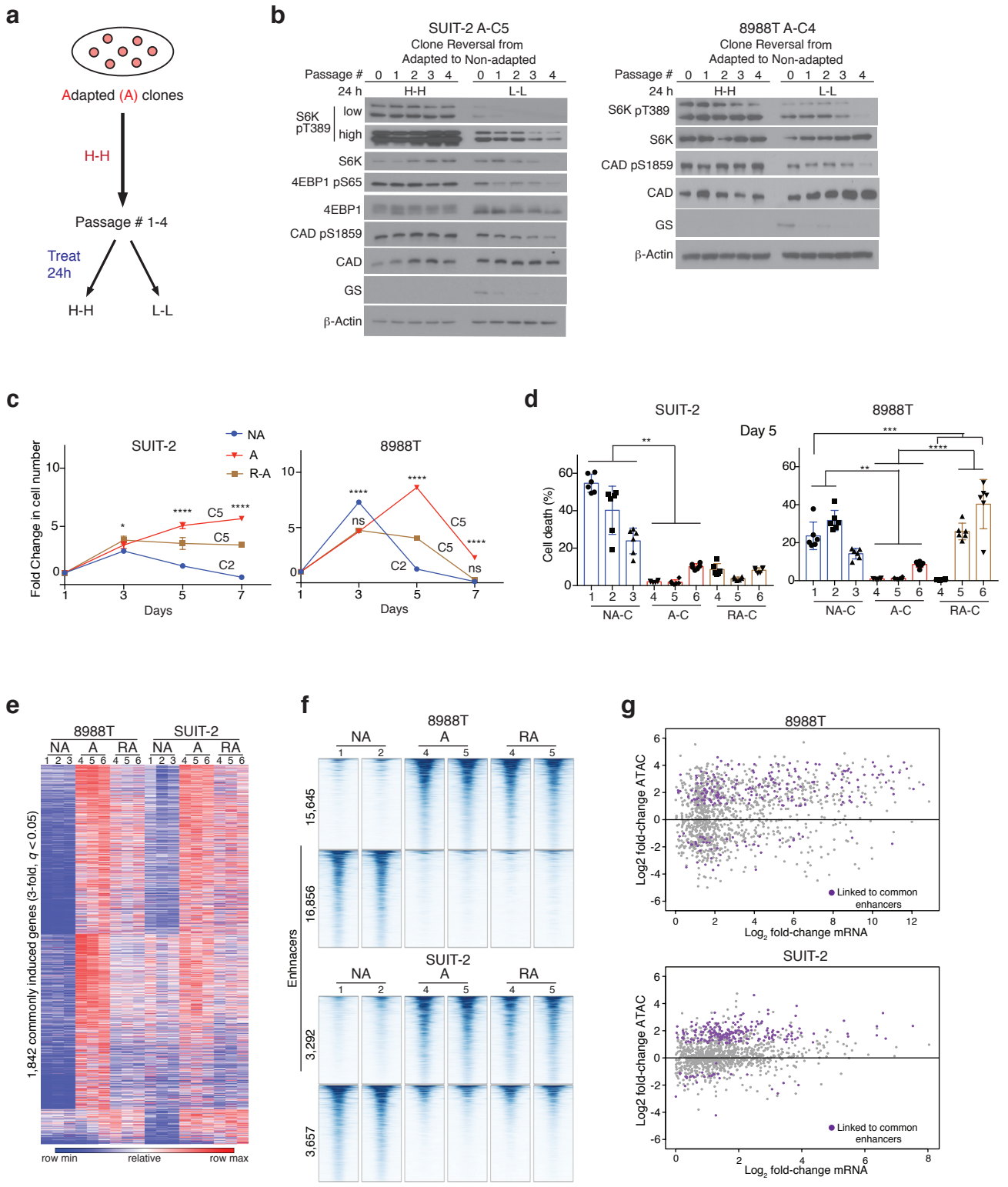
a
Adapted (A) clones
H-H
Passage # 1-4
Treat 24h
H-H
L-L
b
SUIT-2 A-C5
Clone Reversal from Adapted to Non-adapted
Passage # 0 1 2 3 4 0 1 2 3 4
24 h H-H L-L
S6K pT389 low
S6K pT389 high
S6K
4EBP1 pS65
4EBP1
CAD pS1859
CAD
GS
β-Actin
8988T A-C4
Clone Reversal from Adapted to Non-adapted
Passage # 0 1 2 3 4 0 1 2 3 4
24 h H-H L-L
S6K pT389
S6K
CAD pS1859
CAD
GS
β-Actin
c
SUIT-2
8988T
NA
A
R-A
Fold Change in cell number
Days
C5
C2
ns
d
SUIT-2
8988T
Day 5
Cell death (%)
NA-C
A-C
RA-C
e
8988T
SUIT-2
NA A RA NA A RA
1,842 commonly induced genes (3-fold, q < 0.05)
row min
relative
row max
f
8988T
SUIT-2
NA
A
RA
Enhnacers
15,645
16,856
3,292
3,657
g
8988T
SUIT-2
Log2 fold-change ATAC
Log2 fold-change mRNA
Linked to common enhancers

Figure 5

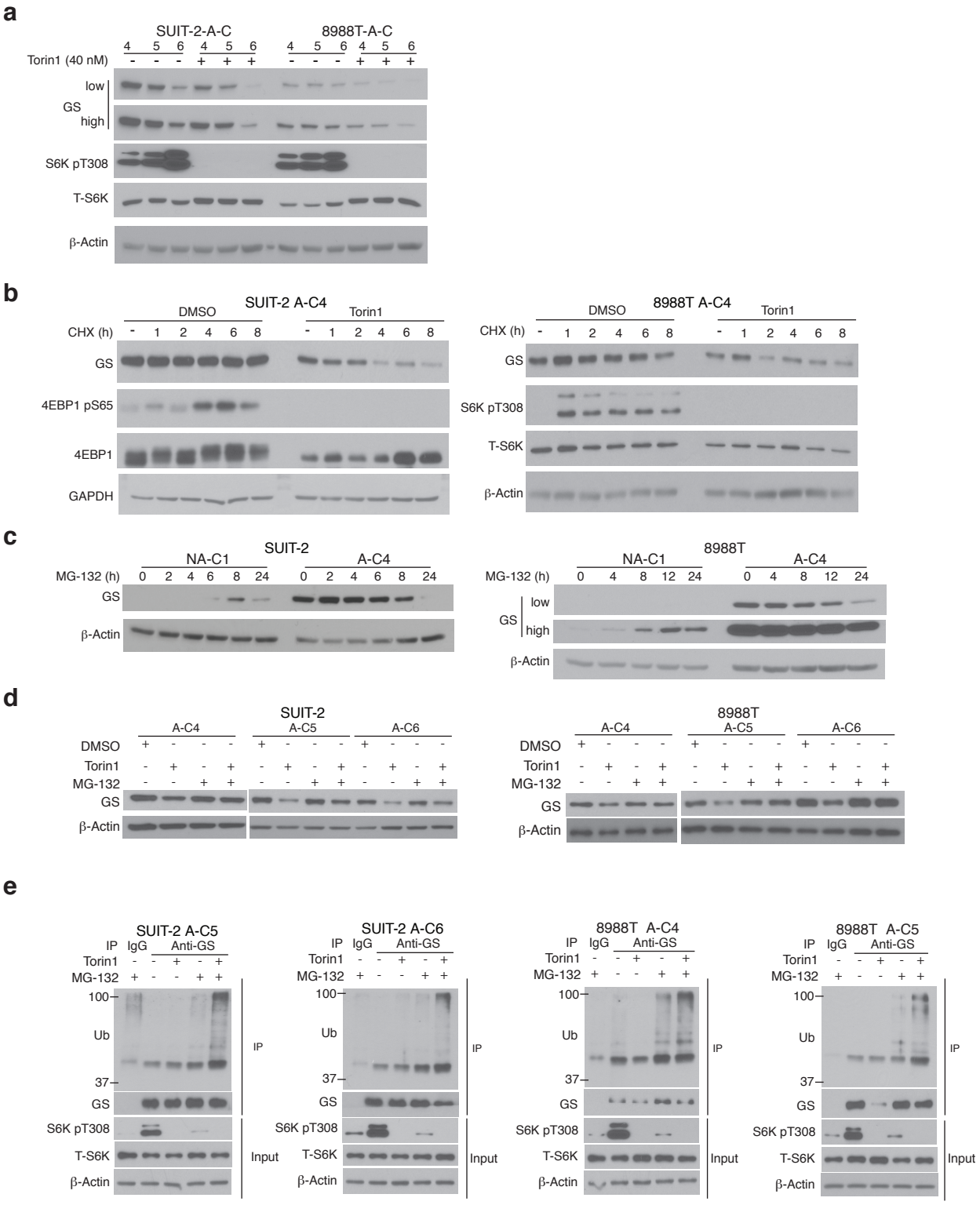
a
SUIT-2-A-C
8988T-A-C
4 5 6 4 5 6
4 5 6 4 5 6
Torin1 (40 nM)
- - - + + +
- - - + + +
GS
low
high
S6K pT308
T-S6K
β-Actin
b
SUIT-2 A-C4
8988T A-C4
DMSO
Torin1
CHX (h)
- 1 2 4 6 8
- 1 2 4 6 8
GS
4EBP1 pS65
4EBP1
GAPDH
S6K pT308
T-S6K
β-Actin
c
SUIT-2
8988T
NA-C1
A-C4
MG-132 (h)
0 2 4 6 8 24
0 4 8 12 24
GS
low
high
β-Actin
d
SUIT-2
8988T
A-C4
A-C5
A-C6
DMSO
Torin1
MG-132
GS
β-Actin
e
SUIT-2 A-C5
SUIT-2 A-C6
8988T A-C4
8988T A-C5
IP
IgG
Anti-GS
Torin1
MG-132
100
Ub
37
GS
S6K pT308
T-S6K
β-Actin
IP
Input

Figure 6

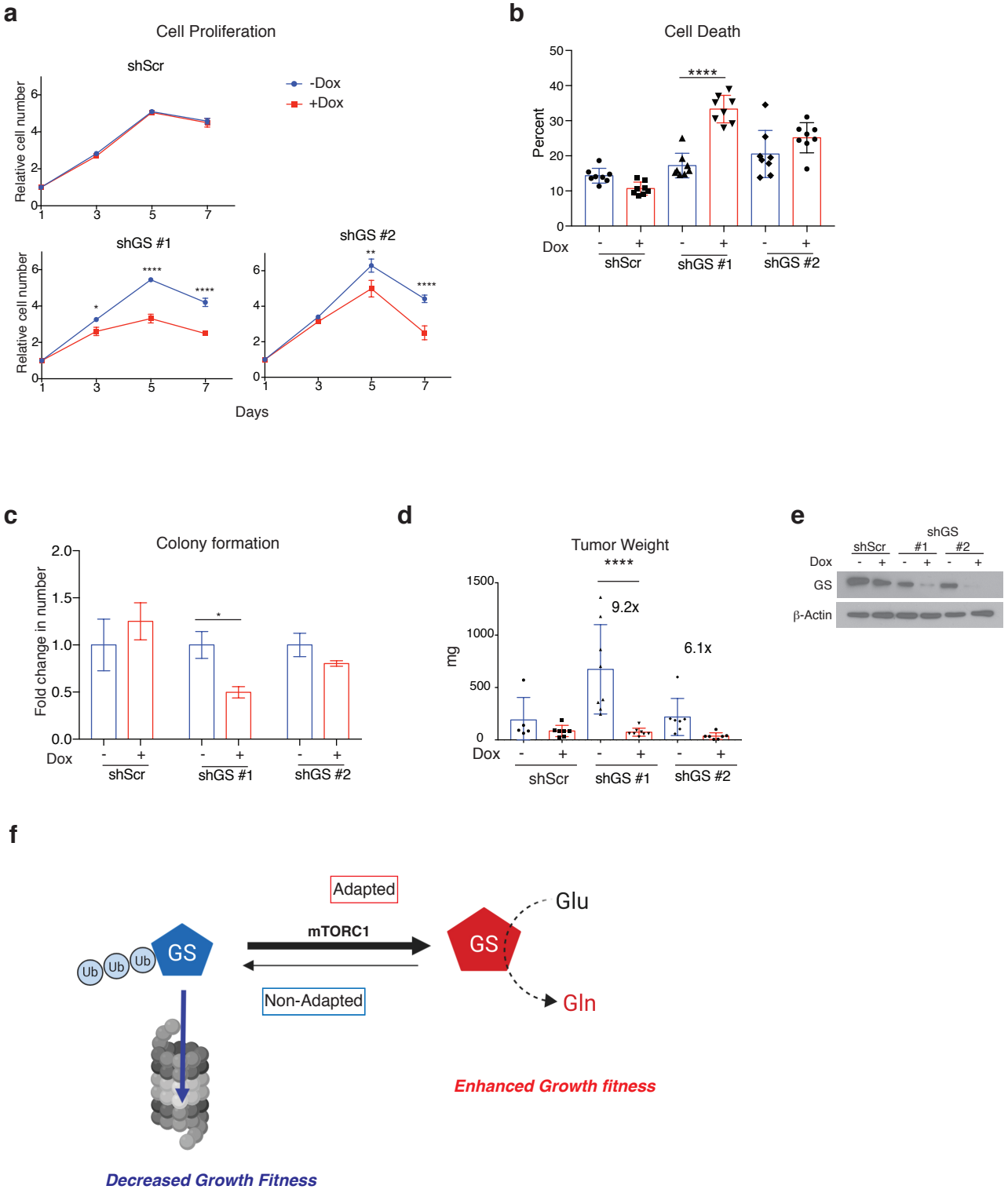
a
Cell Proliferation
shScr
-Dox
+Dox
Relative cell number
shGS #1
shGS #2
Days
b
Cell Death
Percent
Dox
shScr
shGS #1
shGS #2
c
Colony formation
Fold change in number
Dox
shScr
shGS #1
shGS #2
d
Tumor Weight
mg
9.2x
6.1x
Dox
shScr
shGS #1
shGS #2
e
shGS
shScr
#1
#2
Dox
GS
β-Actin
f
Adapted
mTORC1
Non-Adapted
GS
Ub
Glu
Gln
Enhanced Growth fitness
Decreased Growth Fitness

Supplementary Figure 1

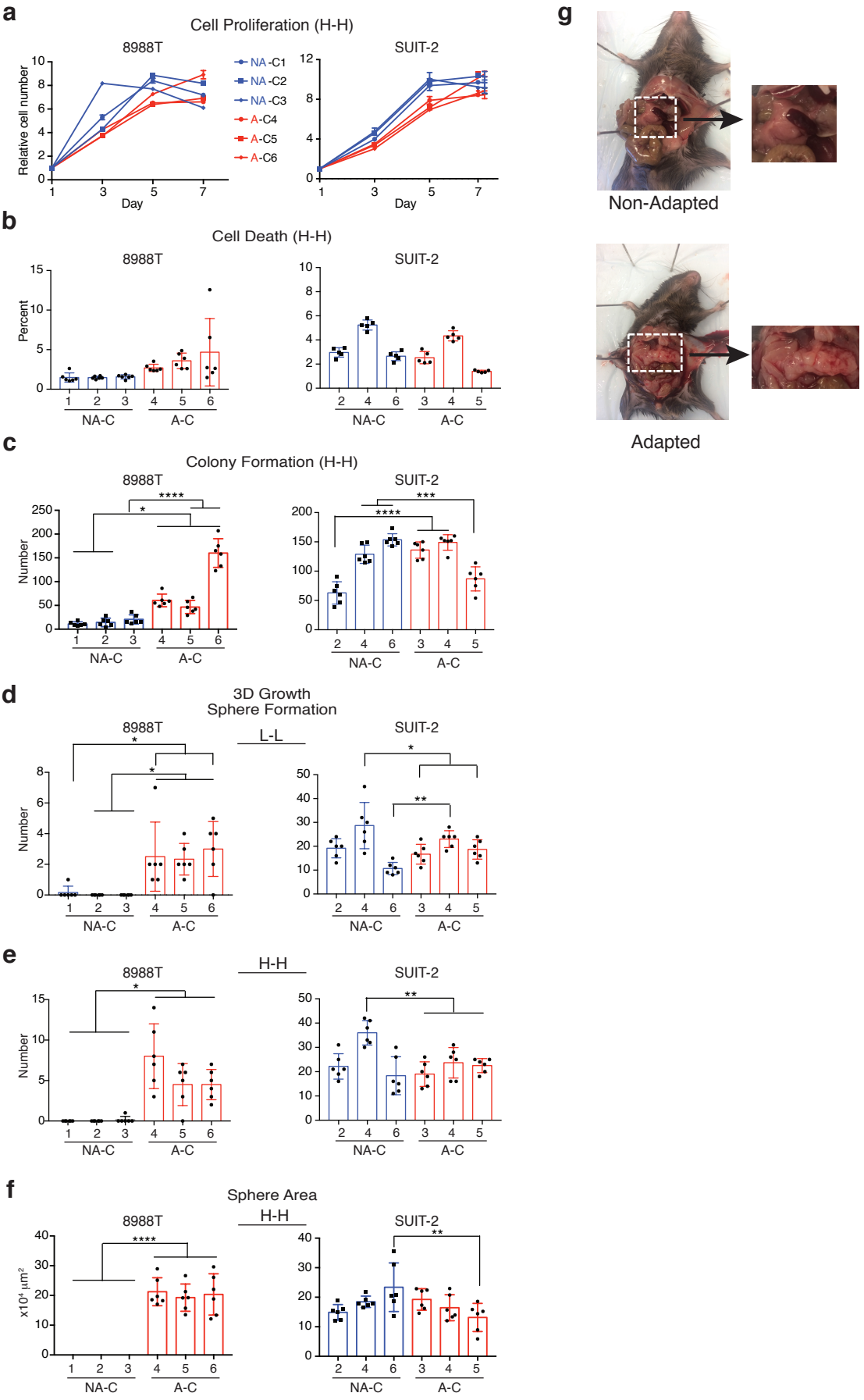

Supplementary Figure 2

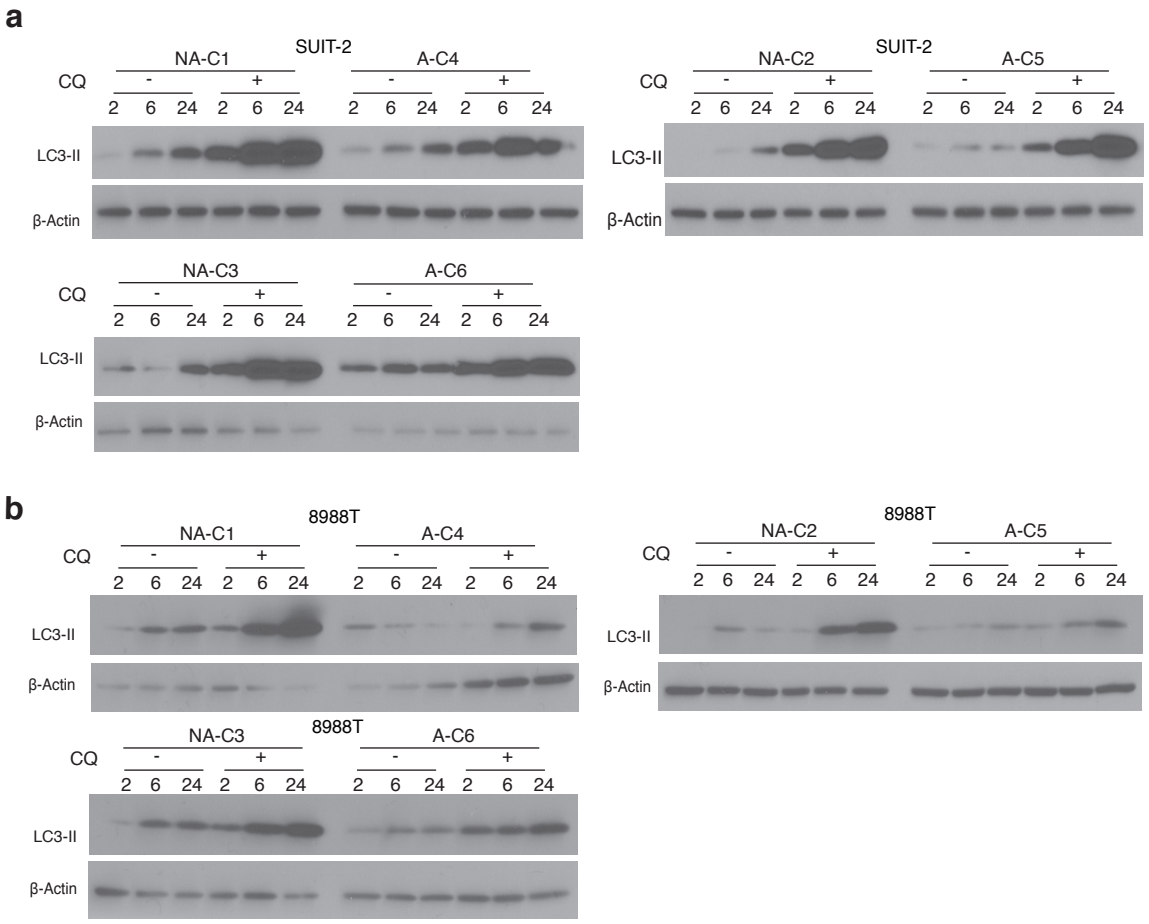

Supplementary Figure 3

a

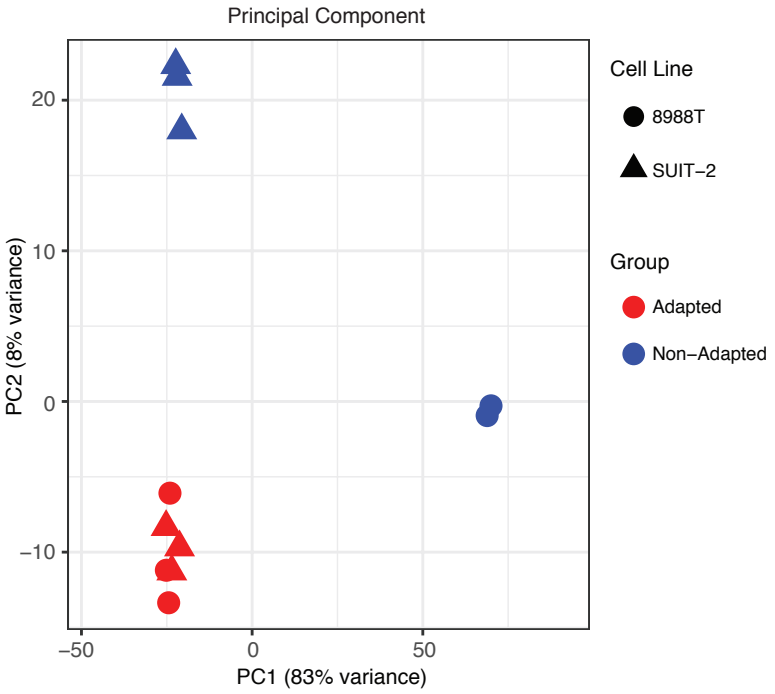

b

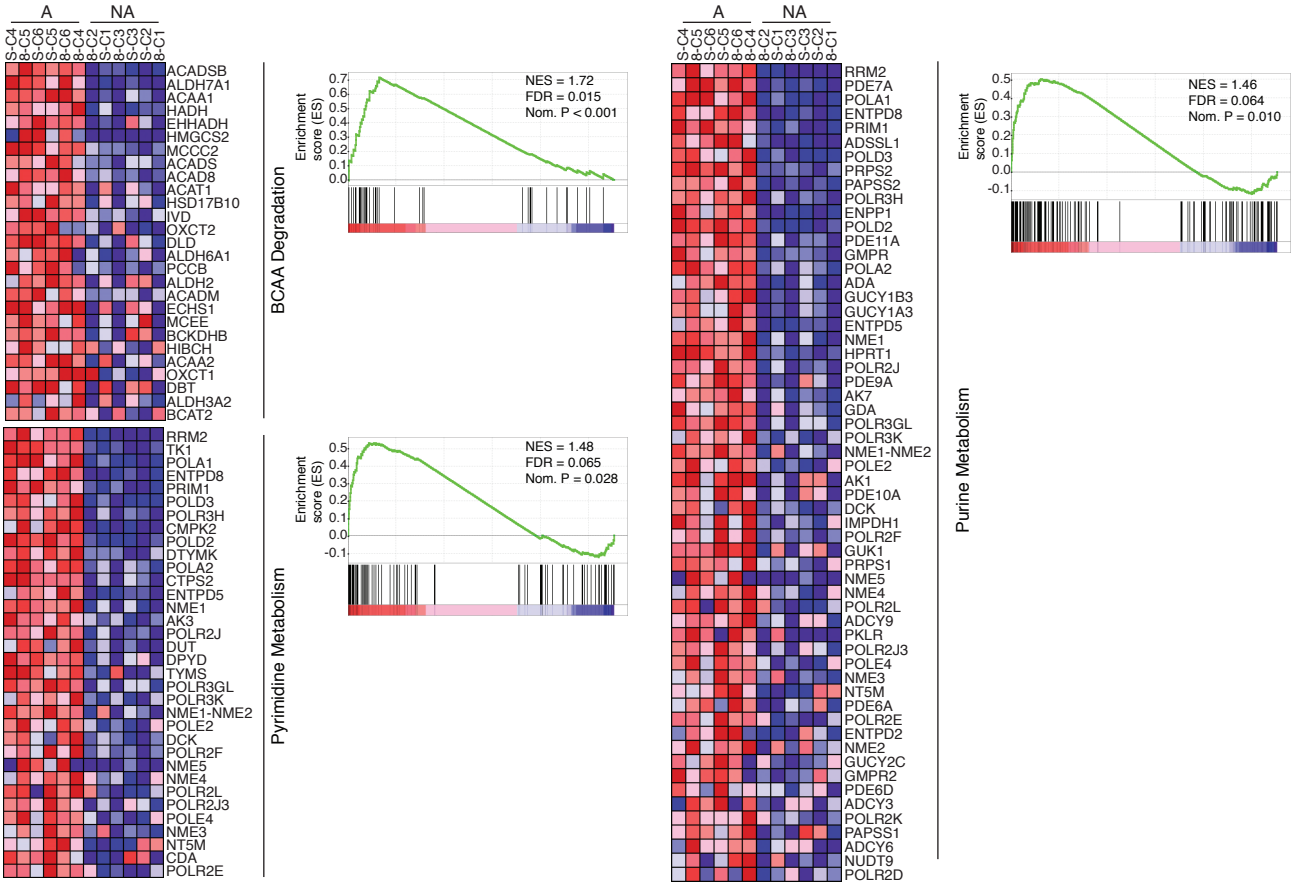

Supplementary Figure 4

a

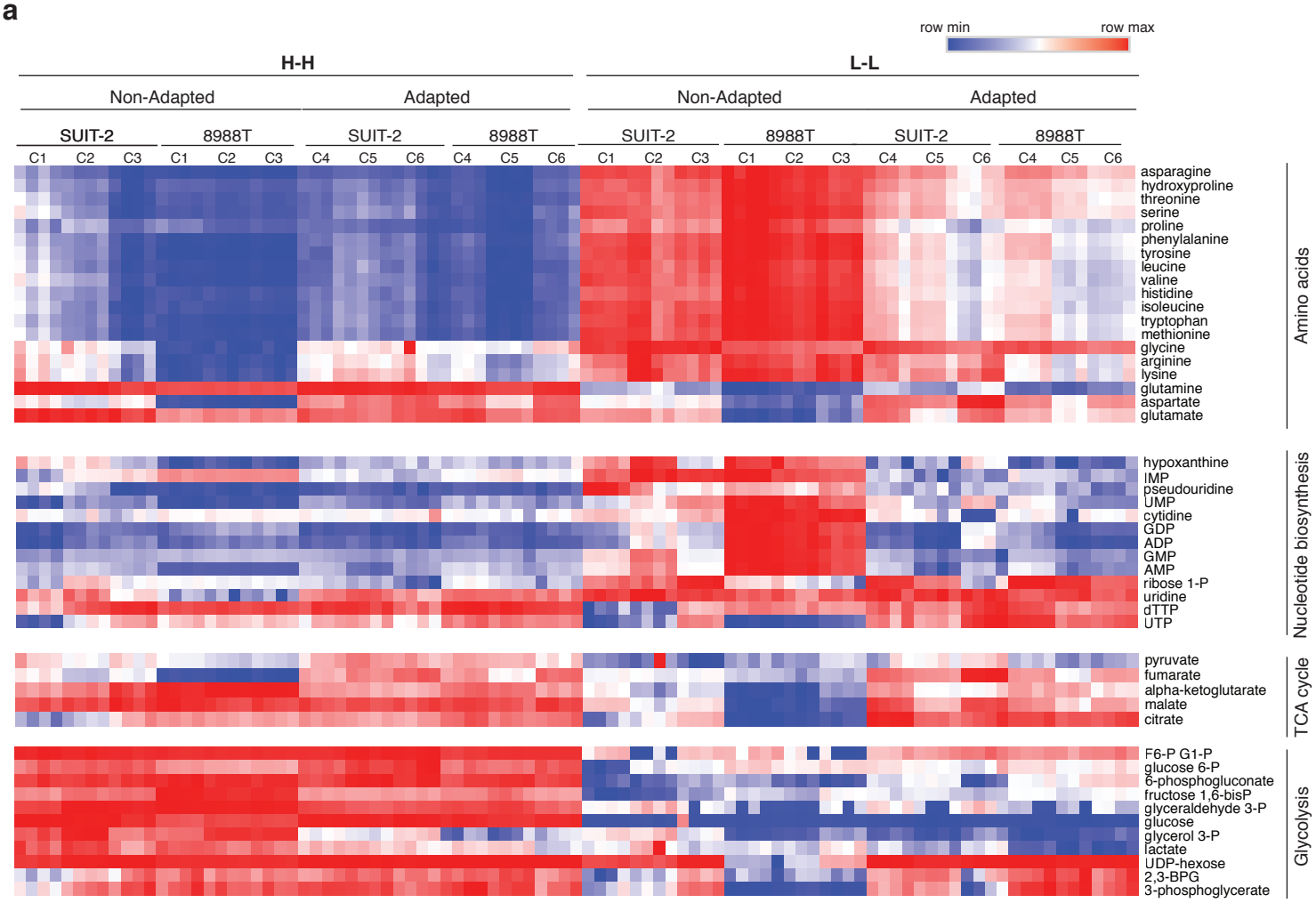

b

Pathways	-log (p)	FDR
Porphyrin and chlorophyll metabolism	5.49E+01	8.85E-23
Phenylalanine metabolism	5.34E+01	2.02E-22
Ubiquinone and other terpenoid-quinone biosynthesis	5.14E+01	9.56E-22
Valine, leucine and isoleucine degradation	**4.95E+01**	**4.57E-21**
Valine, leucine and isoleucine biosynthesis	**4.74E+01**	**3.14E-20**
Aminoacyl-tRNA biosynthesis	4.60E+01	1.07E-19
Phenylalanine, tyrosine and tryptophan biosynthesis	4.44E+01	4.67E-19
Tryptophan metabolism	4.16E+01	6.48E-18
Cyanoamino acid metabolism	4.06E+01	1.52E-17
Sulfur metabolism	3.81E+01	1.64E-16
Arginine and proline metabolism	3.78E+01	2.19E-16
Tyrosine metabolism	3.65E+01	6.84E-16
Propanoate metabolism	3.64E+01	6.84E-16
Nitrogen metabolism	3.62E+01	8.46E-16
Glycine, serine and threonine metabolism	3.58E+01	1.11E-15
Cysteine and methionine metabolism	3.54E+01	1.59E-15
Thiamine metabolism	3.50E+01	2.26E-15
Nicotinate and nicotinamide metabolism	3.40E+01	5.59E-15
Pantothenate and CoA biosynthesis	3.35E+01	8.99E-15
Sphingolipid metabolism	3.23E+01	2.84E-14
Methane metabolism	3.02E+01	2.10E-13
Pyrimidine metabolism	**2.93E+01**	**5.26E-13**
Purine metabolism	**2.64E+01**	**8.51E-12**
Citrate cycle (TCA cycle)	**2.39E+01**	**1.01E-10**
Histidine metabolism	2.34E+01	1.61E-10
D-Arginine and D-ornithine metaoblism	2.26E+01	3.56E-10
Glycolysis and Gluconeogenesis	**2.18E+01**	**7.84E-10**

Supplementary Figure 5

a

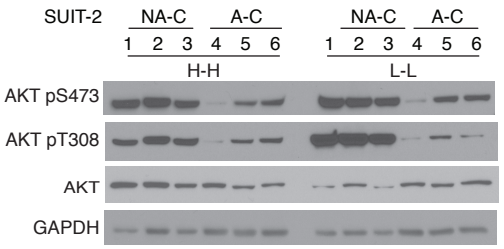

Supplementary Figure 6

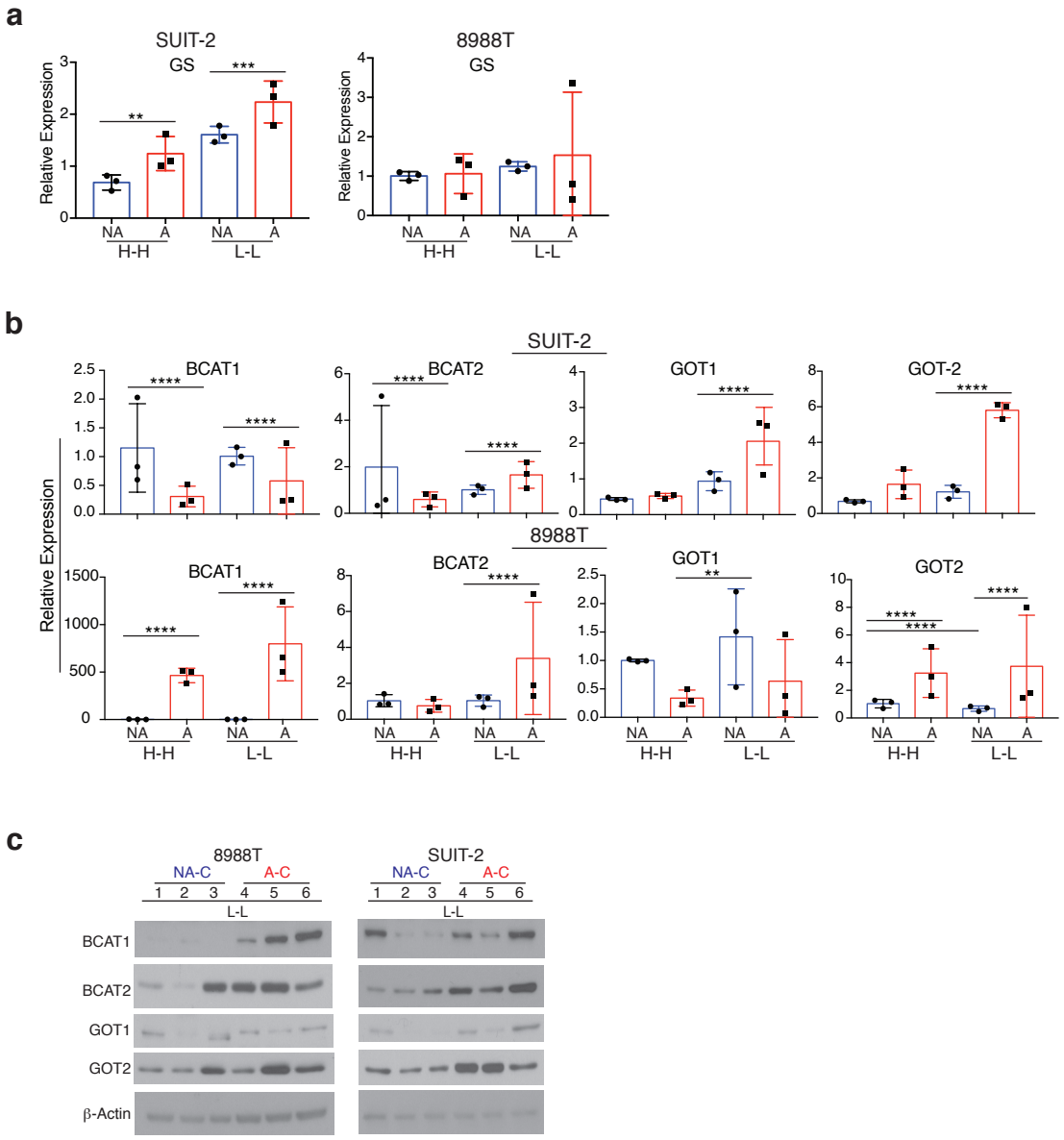

Supplementary Figure 7

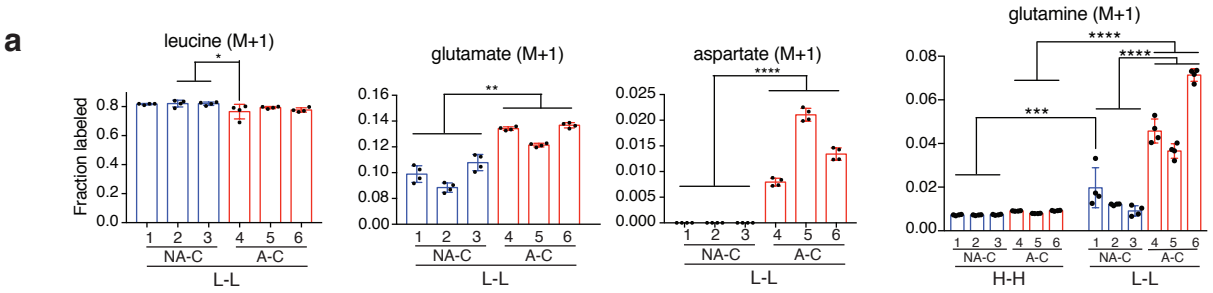

Supplementary Figure 8

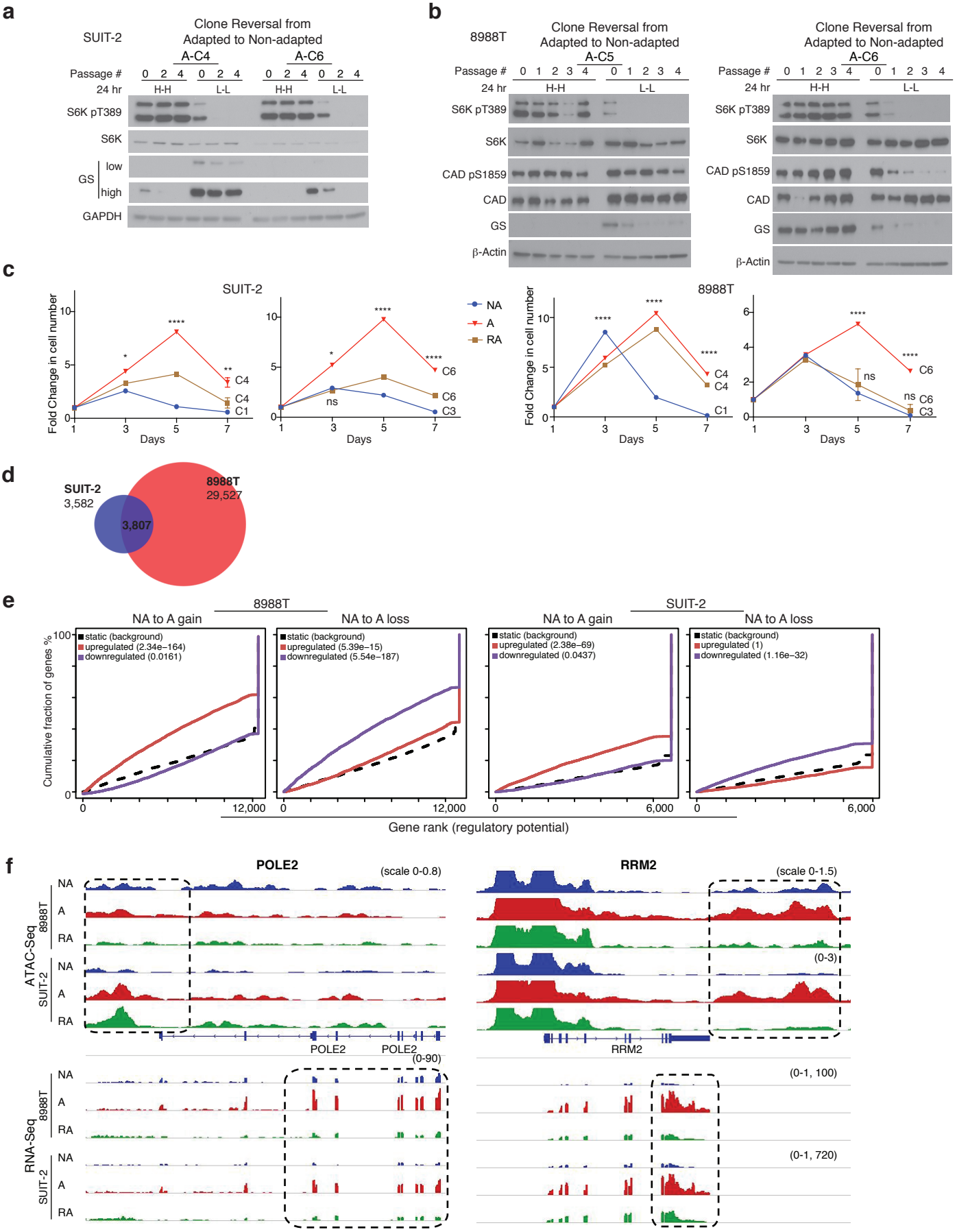

Supplementary Figure 9

a

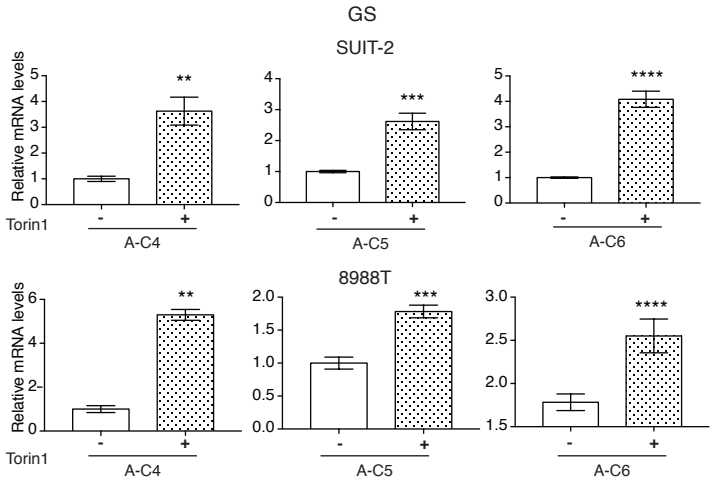

b

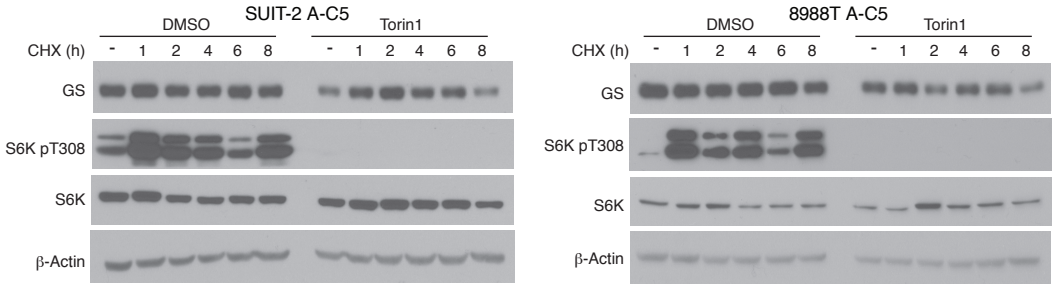

Supplementary Figure 10

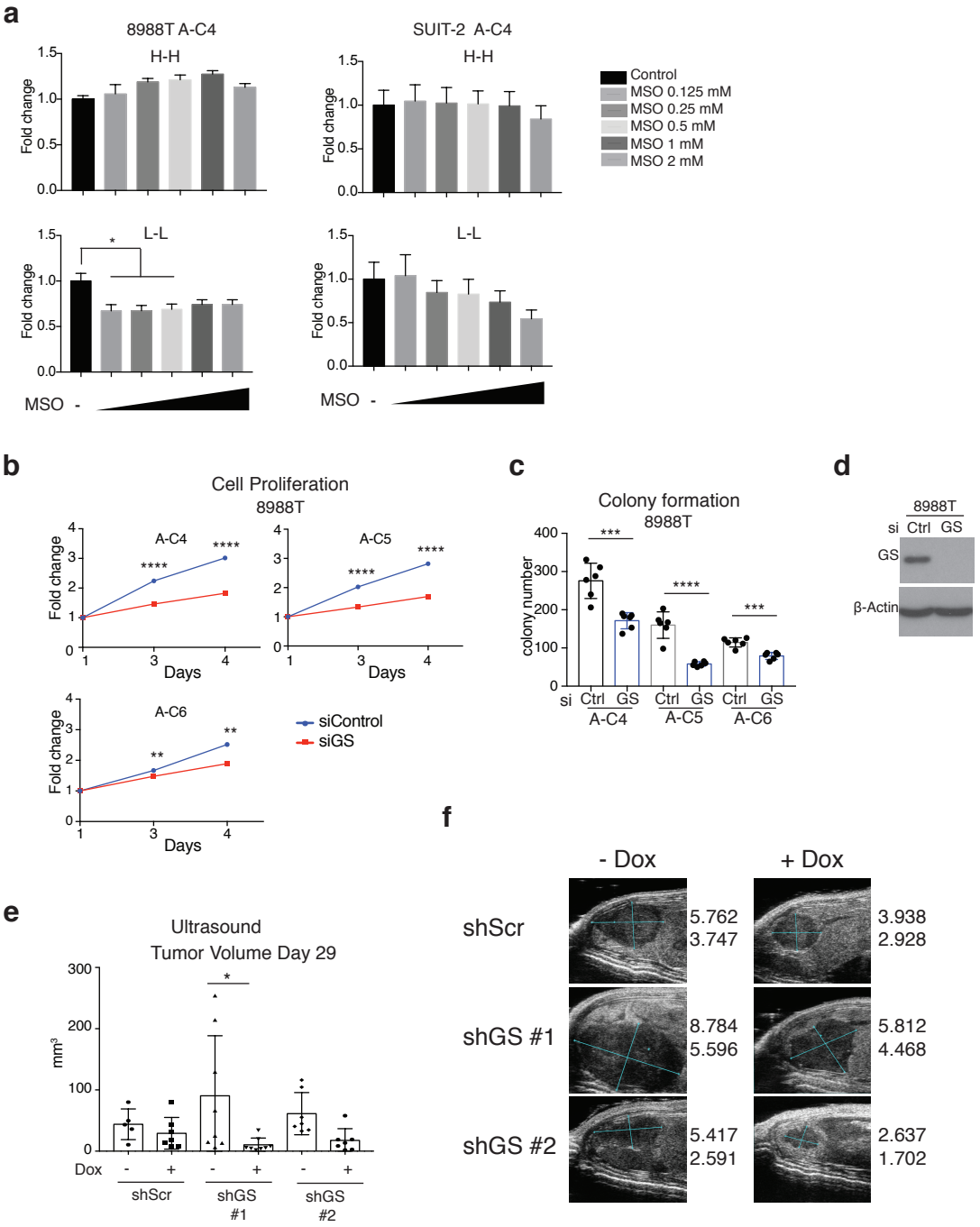

Supplementary Figure 11

a

TMA by pT, pN and grade

Variable	Level	N	Median H-Score	P-value
pT	1	14	150	0.61
	2	89	133	
	3	24	150	
pN	0	32	150	0.34
	1	62	125	
	2	33	150	
Grade	Low	6	195	0.32
	Intermediate	67	138	
	High	52	142	

b

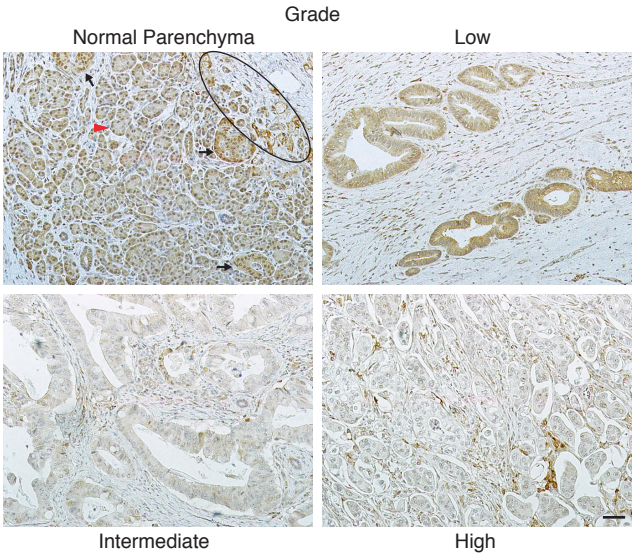
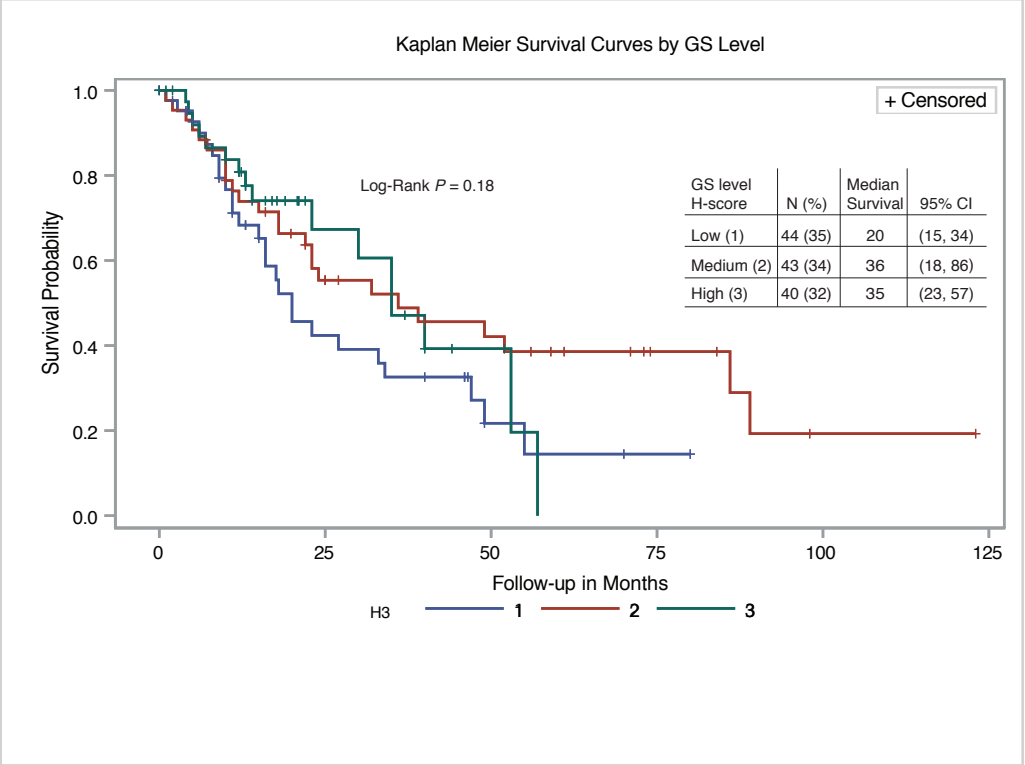
c